Temperature-dependent heating efficiency of magnetic nanoparticles for applications in precision nanomedicine

Temperature-dependent heating efficiency of magnetic nanoparticles for applications in precision nanomedicine

Gabriele Barrera,*[a] Paolo Allia,[a,b] and Paola Tiberto[a]

The power released by magnetic nanoparticles submitted to an alternating driving field is temperature dependent owing to the variation of the fundamental magnetic properties. Therefore, the heating efficiency of magnetic nanoparticles for applications in precision nanomedicine (such as magnetic hyperthermia or heat-assisted drug delivery) can be significantly affected by the local instantaneous temperature of the host medium. A rate equation approach is used to determine the hysteretic properties and the power released by magnetite nanoparticles, and the heat transport equation is solved in a simple geometry with boundary conditions appropriate to both in-lab experiments and *in vivo* applications. Size plays a fundamental role in determining the heating efficiency of magnetic nanoparticles; above a critical size, nanoparticles remain inactive, although they can undergo secondary activation. The experimental conditions for optimal thermal efficiency are expressed by a thermal activity diagram for nanoparticles. In the light of the model's results, features, methods, advantages and dangers of magnetic-particle assisted precision nanomedicine ought to be reconsidered. *In vivo* antitumor applications should take into account the hazards arising from the heat generated by magnetic nanoparticles that diffuse into the neighboring healthy tissue.

1 Introduction

Fundamental and applicative properties of magnetic nanoparticles (NPs) have been a subject of research for a long time [1, 2, 3] and are still actively investigated nowadays [4, 5, 6, 7, 8]. The study of magnetic NPs has been triggered by the remarkable magnetic effects originating from the reduction of size below a critical value [1]. The steadily increasing demand for new functional materials has driven a great number of experimental and theoretical studies on magnetic nanoparticles, whose applications encompass topics such as sensors [9], micromotors [11], environment [12], 3D printing [13]. A number of effects related to particle surface, size distribution, interparticle interaction, tendency to aggregation have been elucidated. A shared picture has finally emerged, stemming from the consolidated knowledge of the basic features of magnetic NPs [10, 4], even if many ill-known parameters may still affect the interpretation of their magnetic properties.

The interest on the behavior of NPs submitted to cyclic magnetization [14] has arisen in correspondence with the rise of interest towards their use in nanomedicine, which is nowadays the most popular macroarea of frontier application of this class of materials [15, 16, 17].

In recent years, the special significance of magnetic NPs or similar nanostrutures in precision nanomedicine has been recognized [18, 19, 20, 21, 22, 23]. In such an innovative practice, nanotechnology helps overcoming treatment resistance of cancer cells by exploiting, e.g., magnetic NPs as diffuse heating agents. Other promising, noninvasive approaches involving thermal energy released by nonmagnetic agents or mechanisms to kill tumor cells, such as phototerapy [25, 26], are being actively studied nowadays. Recently, it has become clear that thermal methods can be usefully complemented by specific chemotherapy, resulting in a synergic enhancement of therapeutic efficiency which may help achieving effective tumor penetration [26].

Magnetic hyperthermia of malignant tissues [24] and heat-assisted antitumor drug delivery using thermoresponsive polymers [27, 28] are based on the properties of properly prepared and targeted magnetic NPs. *In vivo* applications exist:

[a]*INRIM, Advanced Materials Metrology and Life Sciences, Strada delle Cacce 91, I-10135 Torino, Italy. Fax: XX XXXX XXXX; Tel: XX XXXX XXXX; E-mail: xxxx@aaa.bbb.ccc*

[b]*DISAT, Politecnico di Torino, Corso Duca degli Abruzzi 24, I-10129 Torino, Italy.*

† Electronic Supplementary Information (ESI) available: [details of any supplementary information available should be included here]. See DOI: 00.0000/00000000.

‡ Additional footnotes to the title and authors can be included *e.g.* 'Present address:' or 'These authors contributed equally to this work' as above using the symbols: ‡, §, and ¶. Please place the appropriate symbol next to the author's name and include a `\footnotetext` entry in the the correct place in the list.

magnetite NPs with size in the 12-15 nm range have been injected in patients and used in the treatment of malignant tissues under magnetic fields of 2-15 kA/m at the frequency of 100 kHz [29, 30, 17]. Heat generation by magnetic NPs takes place through known dissipation mechanisms (Brown's and Néel's relaxations [31]) in NPs submitted to alternating magnetic fields of sufficently high frequency (up to 100 kHz or more). In this frequency range, the cyclic magnetixation of NPs is hysteretic even if the particles are in the superparamagnetic regime, i.e., when no hysteresis is measured in quasi-static conditions [10].

Ofter real systems contain aggregates of NPs. Aggregation is an effect of interparticle interaction [32, 33] and may give rise in ferrofluids or colloids to various mesostructures such as linear chains and clusters [34, 35]. The effect of aggregation and compactness of aggregates on heating efficiency is far from being clarified: in most cases, a decrease of efficiency with increasing degree of aggregation is either measured [34, 36] or predicted [37, 38]; however, sometimes aggregation can make the heating ability greater [35, 38].

Effects related to NP aggregation are not discussed in this paper, and noninteracting nanoparticles are studied instead; in fact, the spirit of this work is to introduce a simple, but not simplistic intepretation scheme that allows us to highlight how and how much does the temperature behavior of the magnetic properties of NPs influence their heating efficiency, regardless of the degree of aggregation.

The heating efficiency of magnetic nanoparticles is typically measured by their specific loss power (SLP) [31] (also called specific absorption rate (SAR) [39, 40]). Such a quantity is commonly used to quantify the energy conversion efficiency of magnetic nanoparticles in order to help selecting the most effective materials for magnetic hyperthermia applications. This implies that the SLP must provide a most reliable estimate of the thermal performance of a NP system. In the current experimental practice, the SLP is obtained in two rather different ways: *a)* from magnetic-susceptibility measurements, in which the magnetic response of the nanoparticles is assumed to be linearizable [41]; *b)* from the analysis of the temperature variation of the host medium during the first stages of the treatment, so that thermal losses are negligible (adiabatic conditions [39]). In some cases, the SLP has been obtained from the area of the hysteresis loops [42, 43].

The value of the SLP is clearly affected by extrinsic parameters such as particle volume concentration, amplitude and frequency of the driving field, degree of NP aggregation. This quantity has been observed to depend on temperature [44, 45, 42]. However, the SLP must also depend on the intrinsic magnetic properties of the nanoparticles themselves, which directly influence their magnetic losses. This brings about consequences on the heating efficiency which have not been fully elucidated yet and serve as motivation and basis of the present work.The effect of magnetic properties on NP losses is greatest when the energy dissipation is dominated by Néel's relaxation against Brown's; this happens at sufficiently high frequencies [46] ($\approx$ 100 kHz or more) and when the physical degrees of freedom of NPs in space are almost suppressed, as often observed in living tissues [46, 47, 48].

Rate equations are a most effective method to study the hysteretic behavior of uniaxial magnetic NPs described as two-level systems (DWS) [49, 52]. Recently, rate equations have been successfully exploited to describe off-equilibrium properties of magnetic NPs (FC / ZFC curves, hysteresis loops) to a higher degree of accuracy than previous methods [51, 52]and to study their response under non-conventional driving-field waveforms [14]. Rate equations permit to carefully study the features of hysteresis loops of magnetic DWS, including the ones displayed by superparamagnetic NPs at high frequency, which are of greatest interest in today's therapeutic practice [29]. Moreover, they provide a more immediate understanding of the underlying physics with respect to other numerical simulations, and can be applied both to monodisperse and polydisperse systems of nanoparticles whose easy axes randomly point along all directions in space [52].

In the existing literature on the heating properties of magnetic NPs, comparatively little attention has been paid to questions related to the temperature dependence of magnetic parameters such as nanoparticle magnetization and anisotropy [53, 54]. In most cases, the implicit assumption is made that these quantities are not affected by temperature. However, if such an assumption can make sense in a first analysis, the fact that both quantities do depend on temperature in all magnetic nanopartticles should not be disregarded when dealing with applications in which the temperature variation is caused by the nanoparticles themselves.

Aim of this work is precisely to fill this gap. Starting from a simple representation of the temperature dependencies of magnetization and anisotropy, we develop a picture of their effect on the heating properties of magnetic NPs and on the resulting temperature increment produced in an host medium. The rate equations are implemented to determine the power released by Néel's relaxation; the heat transport in the host medium is studied in a spherical, homogeneous sample with different boundary conditions applicable to in-lab experiments and to the therapeutic practice.

It is shown that the temperature dependence of the power released by magnetic NPs has important and somewhat unexpected consequences on the heating efficiency of a NP system; the results strongly depend on particle size. Our results indicate that inaccurate targeting of the NPs can induce notable risks in treated patients.

The present analysis leads one to reconsider the validity of the two classical methods used to obtain the SLP (the linear approach and the adiabatic-condition method). An alternative, sounder method to measure the average power released by magnetic NPs and the SLP is proposed.

2 Magnetic properties: a simple model

2.1 Temperature dependence of NP magnetization and anisotropy

In our model, magnetic NPs are assumed to have a predominant uniaxial anisotropy K_{eff}, so that they can be treated as magnetic double-well systems (DWS) [51, 52]. NPs of size D and

volume $V = (\pi/6)D^3$ carry a magnetic moment $\mu(T) = M_s(T)V$ where $M_s(T)$ is the temperature-dependent saturation magnetization of the material; the temperature-dependent anisotropy is $K_{eff}(T)$. The nanoparticle size is such that the blocking temperature $T_B \simeq K_{eff}V/25k_B$ is well below room temperature T_R (= 300 K). The following room-temperature values of magnetic parameters appropriate to magnetite nanoparticles [51] will be used: $M_s(T_R) = 350$ emu/cm^3 (3.5×10^5A/m); $K_{eff}(T_R) = 4 \times 10^5$ erg/cm^3 (4×10^4 J/m^3). For the sake of simplicity, the ensuing analysis refers to sets of noninteracting, monodisperse particles of size D with easy directions distributed at random. The focus on monodisperse systems is in line with the aim of this work, where temperature-dependent thermal power of magnetic nanoparticles is analyzed in detail. In actual applications, nanoparticle systems are typically characterized by a distribution of sizes. However, when the NPs do not interact or are weakly interacting, the heating effect of a polydisperse system is easily obtained by the weighted sum of the effects of its monodisperse components.

The temperature dependence of both magnetization and magnetic anisotropy in magnetite nanoparticles is little known from actual measurements, particularly above room temperature. In fact, the emphasis of both theoretical and experimental papers on nanoparticles for magnetic hyperthermia is predominantly on the low-temperature behavior of magnetization and magnetic anisotropy (see, e.g., [55]). The region above room temperature is little covered, although in principle the saturation magnetization is easily measurable at high temperature also. Nevertheless, comparatively few papers are focussed on the region between room temperature and the Curie point [56, 57, 58]. On the other hand, magnetic anisotropy and its temperature variation cannot be directly measured in magnetic nanoparticles, and are usually estimated through indirect methods applied below room temperature [55] .

Existing models make use of *ad hoc* expressions for the temperature dependence of M_s, such as the modified Bloch law [59], which however is theoretically unsound at high temperatures. In this paper, the temperature behavior of M_s is taken from Ref. [56] and corresponds to the actual behavior measured in ultrafine magnetite grains [57]. The curve is reported in Figure 1 (black dashed line). The Curie temperature is set to T_C = 856 K in agreement with various experimental data [57, 60, 61]. The uniaxial anisotropy follows the standard power law [59]:

$$\frac{K_{eff}(T)}{K_{eff}(T_R)} = \left[\frac{M_s(T)}{M_s(T_R)}\right]^3; \qquad (1)$$

this curve is also shown in Figure 1 (red dashed line). It should be noted that changing either the shape of the $M_s(T)$ curve or the temperature dependence of magnetic anisotropy is expected to change the quantitative details of the results without affecting the conclusions of this study.

2.2 Temperature dependence of hysteresis loops and released power

Rate equations are a most natural way to get an adequate picture of the behavior of a magnetic DWS submitted to a static or dynamical magnetic field, both at equilibrium and off-equilibrium [49, 50, 51, 52, 14]. In particular, they have been applied to determine the shape of hysteresis loops generated by a high-frequency magnetizing field, both below [52] and above [14] blocking temperature. The method assumes thermally assisted (Arrhenius) NP magnetization reversal [10], the relaxation time for a particle of volume V at zero applied field being:

$$\tau = \tau_0 e^{\frac{K_{eff}V}{k_BT}}, \qquad (2)$$

where $\tau_0 \approx 10^{-9}$ s.

The rate-equation approach permits an accurate description of the effects stemming from the redistribution of magnetic moments in the energy wells by effect of temperature and/or magnetic field. For magnetic nanoparticles, rate equations emerge from the Fokker-Planck equation [62] under the proviso that the ratio $K_{eff}V/k_BT$ be $>>1$; therefore, the validity of the approach depends on temperature, magnetic anisotropy and NP size [14]. With the K_{eff} curve reported in Figure 1a such a condition is fulfilled at (all temperatures) when $D \gtrsim 11$ nm; as a consequence, in most cases the smallest NP size investigated in this work is D = 12 nm. Details about the rate equations used in this paper are given as Supplementary Material. The driving field frequency f is set to 1×10^5 Hz, i.e., well below the upper limit of validity of the method ($\approx 1 \times 10^7$ Hz) [14]. A general discussion about all limits of validity of the rate equation approach can be found in Ref. [52]. The frequency used here is perfectly compatible with the usual experimental practice, both *in vitro* [63, 64] and *in vivo* [65, 17].

In *in vivo* applications of NP-assisted heating of tissues, the product $H_V f$ (where H_V is the vertex field of a minor symmetric hysteresis loop) must not exceed some upper limits which have been considered in the literature [66, 31]. In order not to overcome the limit established in Ref. [31], H_V should not be higher than 600 Oe (47.7 kA/m) at $f = 1 \times 10^5$ Hz. Here, the maximum vertex field is kept at 200 Oe (15.9 kA/m).

Minor symmetric hysteresis loops of monodisperse random NP systems are shown in Figure 1b at different temperatures for two particle diameters (H_V = 100 Oe (7.96 kA/m)). Note that different temperature intervals have been taken for the two diameters, in order to highlight the region where the width of the loops displays maximum amplitude and maximum variation (outside these intervals, the loops are so narrow that the enclosed area becomes vanishingly small). Such a temperature interval depends on NP size.

The most interesting feature of these loops is the non-monotonic temperature behavior of shape and enclosed area A_L. In particular, a sharp maximum of A_L appears between T_R and T_C, its position being strongly dependent on D. The power released by the NPs is just $P_{in}(T) = A_L f$ and is reported in Figure 1c in SI units for different values of D. The temperature where P_{in} is a maximum (T_{MAX}) can be predicted considering that the largest loop area occurs when the typical time of jump across the DWS barrier $\tau(T)$ becomes equal to the time $1/(2f)$ taken to reverse the driving field:

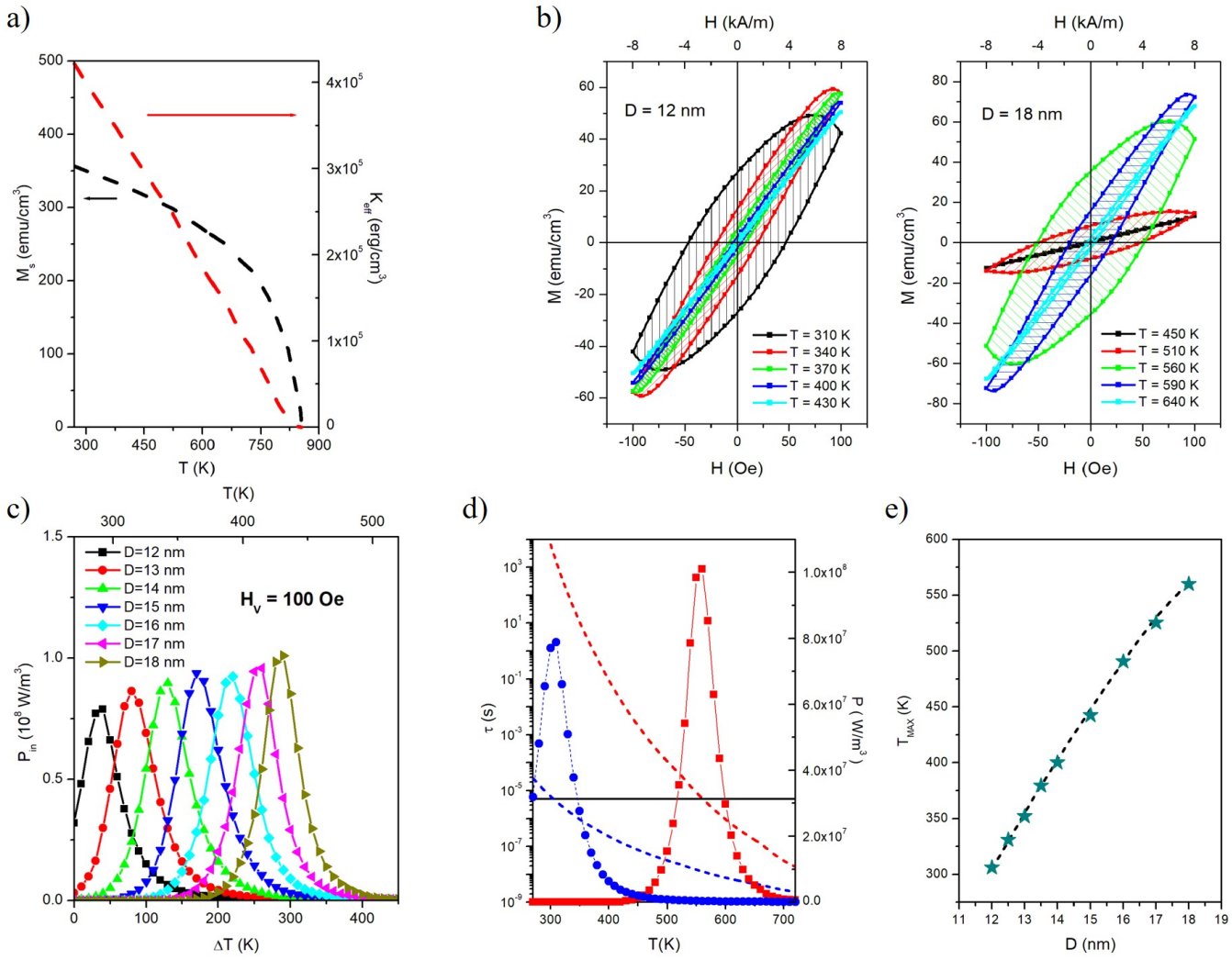

Fig. 1 *(a)* Temperature behavior of spontaneous magnetization M_s and uniaxial anisotropy K_{eff} of the model system (black / red lines, respectively); *(b)* hysteresis loops obtained at different temperatures from the rate equations for two nanoparticle diameters; *(c)* temperature dependence of the power P_{in} released by NPs of different size; ΔT is the temperature increment above the starting temperature (270 K in this case) ; *(d)* comparison between P_{in} curves (connected symbols) and relaxation times τ (dashed lines) for two NP sizes (blue lines: $D = 12$ nm; red lines: $D = 18$ nm); the $1/(2f)$ threshold is reported as an horizontal black line; *(e)* Temperature of the maximum of the $P_{in}(T)$ curve as a function of D. Symbols: data taken from hysteresis loop analysis; dashed line: Equation 4.

$$\tau(T) = \tau_0 e^{\frac{K_{eff}V}{k_B T}} = \frac{1}{2f}. \quad (3)$$

As a consequence, T_{MAX} is found solving the implicit equation:

$$T_{MAX} = \frac{\pi D^3}{6k_B ln(\frac{1}{2f\tau_0})} K_{eff}(T_{MAX}) \quad (4)$$

The validity of this prediction is checked in Figures 1d and 1e. Figure 1d shows the temperature behavior of $\tau(T)$ for D =12 / 18 nm (blue / red dashed lines, respectively); these curves cross the $1/(2f)$ line exactly where the corresponding released power shows the peak (blue / red connected symbols, respectively). The agreement between calculated and predicted T_{MAX} values (dashed line and symbols, respectively) is shown in 1e and is very good for all diameters.

The condition reported in Eq.(3) can be undestood considering that when $\tau << 1/(2f)$ the DWS are very close to thermal equilibrium and the hysteresis loop is very narrow; on the contrary, when $\tau >> 1/(2f)$ the redistribution of magnetic monents in the energy wells is almost suppressed, and the magnetization only rotates towards the field direction giving rise to a nearly anhysteretic curve. Only when $\tau \approx 1/(2f)$ does the redistribution most effectively keep the DWS out of equilibrium as the loop is being performed, resulting in the largest enclosed area. A more quantitative discussion is given in Section 3.4.

2.3 Comparison with the linear expression of released power

The quantity $P_{in}(T)$ evaluated by solving the rate equations for the DWS can be compared with the analytical expression of the power dissipation by a system of noninteracting nanoparticles, developed in the strictly linear regime [41]; in SI units:

$$P_{LIN}(T) = \pi\mu_0^2 \frac{M_s^2(T)V}{3k_B T} H_V^2 f \frac{2\pi f\tau(T)}{1+(2\pi f\tau(T))^2} \quad (5)$$

This expression predicts a temperature dependence of the power dissipation bearing qualitative similarities with the trend we obtain from rate equations; in particular, a peak of P_{LIN} appears as a function of temperature by effect of the presence of the Lorentzian term in Equation 5. However, there are strong quantitative difference between the outputs of the two methods, mainly related to the fact that for finite values of the vertex field the linear approximation leading to Equation 5 is no longer appropriate, as discussed in Appendix A.

3 Heat generation

3.1 Heat transfer equation

The rate equation model gives the heating power of a magnetic NP system. On the other hand, *in vivo* applications need the knowledge of the temperature increment in the region containing the particles. A further step is therefore needed to describe how the heating power results in a temperature increment. This is typically done by introducing a heat equation with internal power generation, tailored to depict as accurately as possible the processes of heat transport in complex systems. The validity of the heat equation can be checked by comparison with actual temperature measurements conducted on suitable phantoms and/or animal models. In fact, all equations governing heat diffusion in living tissues (Pennes' and other bioheat equations [67]) are *ad hoc* specializations of the classical Fourier equation, suitably shaped to include the main heat transfer mechanisms and heat sources in living bodies. In the spirit of developing a model as simple as possible, the standard time-dependent Fourier equation with internal heat source is used in this paper. This is justified by the laboratory or *in vitro* applications envisaged here. However, the results can be exported to *in vivo* applications also by using suitable boundary conditions (see Subsection 3.3).

For the sake of simplicity the Fourier equation is solved in radial symmetry, as done in other papers [54, 68]. The system analyzed here is depicted in Figure 2 and consists of a sphere of radius b =0.01 m filled with a homogeneus medium (a biological simulant, such as a tissue phantom) containing a space- and time-dependent heat source. The equation is:

$$\frac{\partial^2 T(r,t)}{\partial r^2} + \frac{2}{r}\frac{\partial T(r,t)}{\partial r} + \frac{P_{in}(T)}{k} = \frac{1}{\alpha}\frac{\partial T(r,T)}{\partial t} \quad (6)$$

where $P_{in}(T)$ is the power generated by the homogeneous distribution of NPs in the phantom; in general, such a quantity depends on both r and t through the local temperature $T(r,t)$. In this model, both thermal conductivity k and thermal diffusivity α are considered uniform and constant; their values are k =0.5 W/mK (appropriate to typical tissue simulants [69, 70] and $\alpha = 1.4\times10^{-7}$m^2/s .

The only mechanism of heat generation considered here is Néel's relaxation in magnetic NPs, because: i) at the frequency of interest, Brown's relaxation is negligible with respect to Néel's [46]; ii) in living tissues or tissue phantoms NP translation and rotation often are almost suppressed[46, 47, 48].

3.2 NP heating of a medium as a cumulative effect

It should be noted that the temperature of a medium initially at equilibrium at $T = T_0$ is not affected at all by the magnetic power released by a *single* NP [71]. Moreover, the temperature of such a nanoparticle would not increase from T_0, the heat generated being immediately lost to the surrounding medium which would act as a perfect heat sink. In fact, substantial heating of the host medium does occur by the cumulative effect of many independent NP dispersed in it, viewed as pointlike heat sources. When the volume fraction of magnetic NPs in the medium is f_V and the power released by a single NP is P_{in}^{l} (per unit volume of *magnetic material*), the overall power released by an ensemble of homogeneously distributed NPs is $P_{in} = f_V P_{in}^{\mathrm{l}}$ (per unit volume of the *host medium*).

Therefore, a homogeneous dispersion of NPs in the phantom produces a power density uniformly distributed within the sherical sample. Such a power is able to efficiently heat the host medium, also heating the magnetic nanoparticles embedded in it. One makes the simplifying hypothesis that each nanoparticle is instantaneously in thermal equilibrium with the immediate sur-

roundings and that the temperature inside each particle is always uniform. These assumptions are fully justified by the small size of the particles. As a consequence, the temperature of a nanoparticle at a distance r from the center of the sphere changes as $T(r,t)$ and the arguments of Section 2.2 apply.

3.3 Boundary conditions

In this work, the following boundary conditions (BCs) will be used:

a) the heated sample is thought as immersed in a ice-water thermostat. The BC is:

$$T(b,t) = T_0 \qquad (\textbf{BC:T}) \tag{7}$$

where T_0 =273 K. The initial temperature of the phantom is $T(r,0) = T_0$; see Figure 2a;

b) the phantom is immersed in a non-thermostatic medium towards which the energy is vehiculated through a convective heat flux mimicking the typical process in living tissues (in that case, the heat generated by a distributed source is effectively removed by tissue-blood perfusion, whose effect greatly varies from tissue to tissue [72, 73, 74, 75, 76, 77]). The BC is:

$$\frac{\partial T(r,t)}{\partial r}\Big|_b = -\frac{h}{k}T(b,t) \qquad (\textbf{BC:C}) \tag{8}$$

where h is the convective heat transfer coefficient (in W/m^{2}K). The initial temperature of the phantom is $T(r,0) = T_0$ with T_0 =310 K; see Figure 2d.

The parameter h is directly related to the product $[Wc_b]$ of Pennes' equation [67] (where W is the local tissue-blood perfusion rate (in Kg/m^{3}s) and c_b the blood's specific heat (in J/KgK)). Considering the heat removed by blood perfusion from the surface of a sphere of radius b, the following relation is easily derived:

$$h = \frac{b[Wc_b]}{3}; \tag{9}$$

3.4 Typical solutions with temperature-dependent input power

Equation 6 with the temperature-dependent heat source is solved by a standard finite difference method; at each time step and for all r values the input power P_{in} is updated to the instantaneous value of T, according to the curves given in Figure 1c. Solving the Fourier equation with the appropriate BC gives the temperature increment $\Delta T(r,t)$.

Typical examples are shown in Figure 2b,c for the thermostatic boundary condition with a vertex field of 100 Oe; the stationary solutions obtained for different NP sizes are given in Figure 2b; the time evolution of the temperature increment in $r = b/2 = 5\times10^{-3}$ m is reported in Figure 2c for the same diameters. The curves have been calculated for two values of f_V close to the actual volume concentration of magnetite NPs in practical therapy applications [29] (112 mg/ml, equivalent to $f_V = 8.4\times10^{-3}$). The corresponding solutions obtained for the convective boundary condition are reported in Figure 2e,f.

It should be noted that both absolute value and space profile of the temperature increment within the heated sphere depend on its radius b. For instance, under convective boundary conditions the temperature at the center ($r = 0$) increases with the sphere radius b according to a quadratic law of the type $A + Bb^2$ where A, B are constants given by the model, whereas the temperature at the boundary ($r = b$) is independent of the value of b and equal to the constant A. As a consequence, when b is very small, the temperature inside the sphere becomes almost constant and close to A. With the parameters of Figure 2 this happens when $b < 1\times10^{-3}$ m.

On the other hand, when b is on the centimeter scale as in the case examined here, under both boundary conditions the temperature increments turn out to be strongly dependent on NP size and f_V, and can be rather strong; the optimum target temperature can always be easily attained by properly tuning both H_V and f_V. The effect of NP diameter on the final ΔT value in r =0 is shown in Figure 3a for two values of H_V. The heating efficiency is very sensitve to the NP size; actually, a sharp maximum of ΔT as a function of D is expected for all values of H_V; however, such a maximum appears in just one case in Figure 3, being displaced below 12 nm (i.e., beyond the limit of validity of our approach) in the remaining cases.

It is possible to predict when a nanoparticle of given size contributes to the heating process, and when it is thermally inactive. As discussed in Section 2.2, thermal efficiency is related to the width of the hysteresis loop. Now, the magnetization of a system of NPs becomes basically anhysteretic (even under a high-frequency driving field) when the relaxation time $\tau(T)$ is either much larger or much smaller than $1/(2f)$: in the first case, the NP system is close to thermal equilibrium, in the second case the degree of occupancy of the two wells is substantially constant. A region of *thermal activity* for a monodisperse NP system can be defined in the diameter-temperature plane, as shown in Figure 3b. The upper/lower boundaries $T_{AH}(D)$ and $T_{AL}(D)$ are determined by requesting, e.g., that $\tau = 0.01/(2f)$ and that $\tau(T) = 100/(2f)$, respectively; they are obtainediny analogy with Equation 4 by solving the implicit equations:

$$\begin{aligned} T_{AH} &= \frac{\pi D^3}{6k_B ln(\frac{0.01}{2f\tau_0})} K_{eff}(T_{AH}) \\ T_{AL} &= \frac{\pi D^3}{6k_B ln(\frac{100}{2f\tau_0})} K_{eff}(T_{AL}). \end{aligned} \tag{10}$$

As shown in Figure 3b, $T_{AH}(D)$ and $T_{AL}(D)$ are the temperatures above and below which the cyclic magnetization of a NP of diameter D becomes nearly anhysteretic (even if for different reasons); the difference $\Delta T_{ACT} = T_{AH} - T_{AL}$ defines the temperature interval where the monodisperse system is thermally active. Of course, the T_{MAX} curve belongs in this region (red dashed line). The horizontal line in Figure 3b marks the starting temperature T_0 of the host medium (in this case, 310 K). If the NP diameter is such that T_{AL} is below that line, the host medium

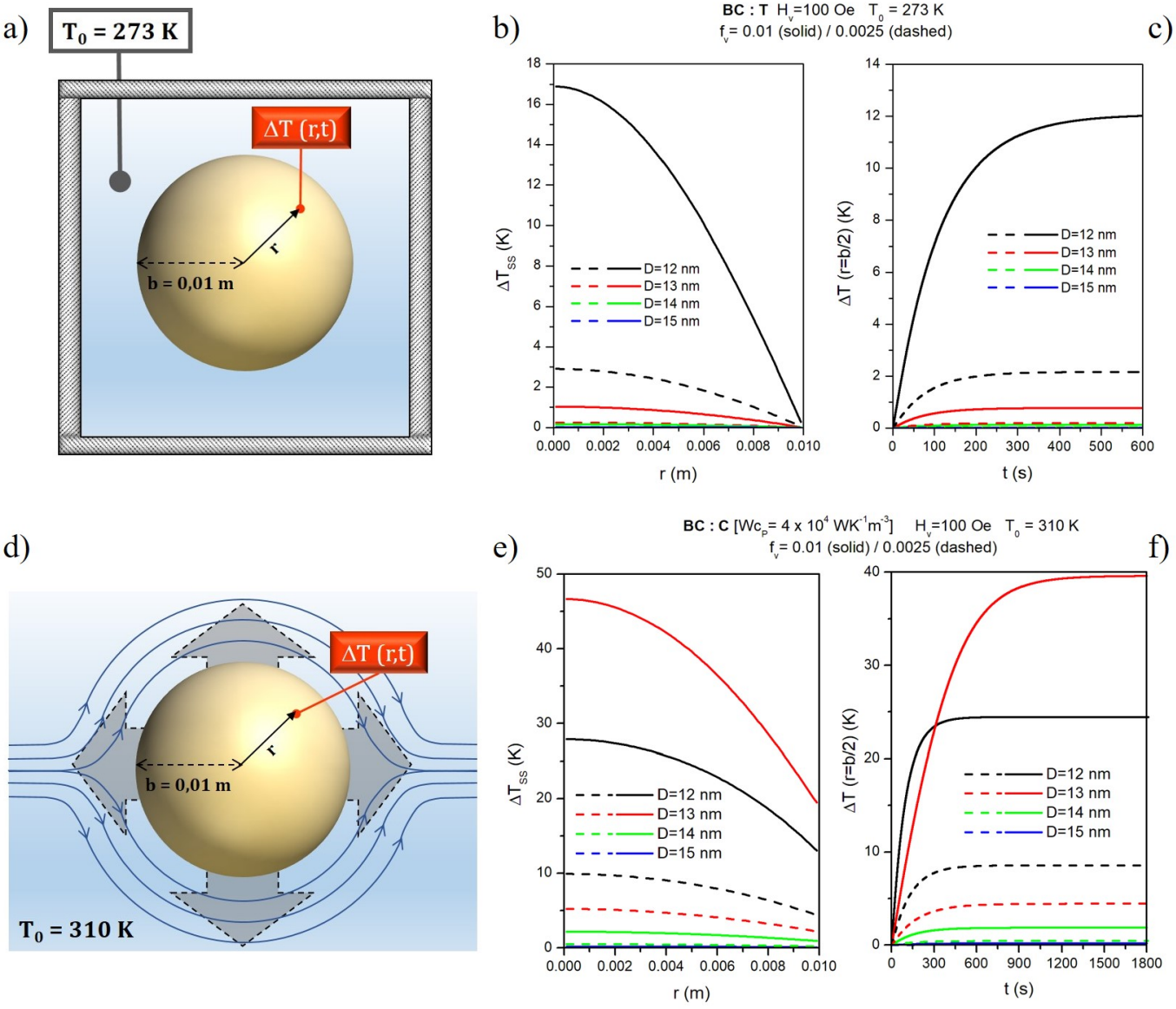

Fig. 2 *(a)* Sketch of the model system in thermostatic boundary conditions (ice-water thermostat); *(b)* space profile of the steady-state temperature increment for different NP diameters (thermostatic BCs); *(c)* time profile of the temperature increment in $r = b/2$ for the same NP diameters (thermostatic BCs); *(d)* sketch of the model system with convective boundary conditions; *(e)* space profile of the steady-state temperature increment for different NP diameters (convective BCs); *(c)* time profile of the temperature increment in $r = b/2$ for the same NP diameters (convective BCs).Note that the temperature increment for $D = 15$ nm is so small that the corresponding lines in panels b, c and e, f are indistiguishable from the $x-$axis on the scale of the figures.

will be heated; if the opposite is true, the host medium will not be heated. In the present case, the $T_{AL}(D)$ curve intersects the T_0 =310 K line immediately above D =14 nm, which explains the behavior of the curves reported in panel *(a)* of the same Figure. Although the quantitative details of the present discussion are based on the special values of magnetic properties used in the present work, the thermal activity diagram of Figure 3b has a general validity and can be easily adapted to other types of magnetic nanoparticles.

In practical applications of magnetic NPs as distributed heating elements in a biological environment, the final average temperature $< T(\infty) >$ is never much higher than T_0 [78, 79]; however, such a target temperature must be very precisely reached, an error of a few degrees being in general detrimental and/or dangerous. One could deduce that in these conditions the magnetic parameters could be safely assumed to be constant, so that the released power would be a constant too. However, this is not the case: replacing a temperature-dependent input power with a constant input power has measurable consequences even for small temperature increments, as illustrated in Appendix B.

3.5 Effect of temperature-dependent input power

3.5.1 Anomalous shape of the T(t) curves

The non-monotonic temperature behavior of the power relased by the NPs is reflected in "anomalous" features of the $\Delta T(r,t)$ curves. Typical examples are shown in Figure 4 where then P_{in} curves are associated with the corresponding time evolution of ΔT for $r = b/2$, obtained for the convective BC, for four different NP diameters (note that the vertical scales are the same in all panels).

Substantial heating of the phantom occurs only for D <15 nm; the maximum final temperature is not a monotonic function of D, as already observed in Figure 3. The shape of the $\Delta T(b/2,t)$ curve exhibits an interesting, anomalous behavior for $D = 14$ nm: the temperature begins to rise with a rather low slope; however, after about 400 s this sharply increases to finally go to zero when the steady state is approached. This is not an exceptional behavior and is intimately related to the shape of the corresponding P_{in}(T) curve.

The heating curves of Figure 4 can be explained with reference to the temperature behavior of the corresponding P_{in} curves (reported in the right panels of the same Figure):
- for $D = 12$ nm, the initial input power (at $T = T_0$ =310 K) is large and the sample temperature begins to rise with a high initial slope (dashed black curve); however, P_{in} gradually decreases with increasing T, so that the steady-state temperature is not very high;
- for $D = 13$ nm, the initial power is comparable to the previous case, so that the initial slope of $\Delta T(b/2,t)$ is very similar (red dashed line); however, now P_{in} increases in a temperature interval above T_0, and the steady-state temperature is much higher than in the previous case.
- for $D = 14$ nm, the initial power is very small, so that the $\Delta T(b/2,t)$ curve starts with a low slope; however, the temperature increment is such that the NPs enter the region of the peak of input power; as a consequence, an extra-heating effect is switched on (corresponding to the sharp increase of the slope of the $\Delta T(b/2,t)$ curve); eventually, a very high steady-state temperature is reached.
- finally, for $D = 15$ nm, the initial power is extremely small, so that the NPs reach a steady-state temperature very far from the region of the peak of input power, and the extra-heating is not switched on. The final temperature increment, in this case, is lower than the one one could predict from the initial slope of the curve.

These examples help recognizing how much it could be misleading to determine the specific loss power (SLP) of a set of nanoparticles and to estimate the resulting maximum temperature from the initial slope of the $\Delta T(t)$ curve, as often done in the literature [39, 40]. Figure 4 clearly shows that the final temperature of two nanoaprticle sets can be markedly different even if the initial heating rate is the same, and that even if one measures temperatures compatible with the therapeutic practice during the initial stages of heating, the complete time evolution of temperature can lead to unexpected results. This point is further treated in Subsection 3.5.2.
It should be stressed that the results discussed here apply to a typical laboratory experiment conducted using parameter values representing a real case of therapeutic hyperthermia. It is not meant as a simulation of an *in vivo* application, but as a concept experiment helping one to better understand the caveats stemming from a doubtful estimate of the heating effect of a set of nanoparticles.

3.5.2 Issues with adiabatic masurements of the SLP

The specific loss power (in W/g) is defined as:

$$W_{SLP} = \frac{input\,power}{mass} = \frac{P_{in}V_s}{m_{NP}} \tag{11}$$

where m_{NP} is the total mass of magnetic nanoparticles and V_s the volume of the sample. In measurements conducted in adiabatic conditions [39], the product $P_{in}V_s$ is given by the initial slope of the heating curve:

$$P_{in}V_s = C\frac{dT}{dt}\Big|_{t\to 0} \tag{12}$$

where C is the thermal capacity of the sample. The steady-state temperature increment ΔT_{SS} is then estimated to be:

$$\Delta T_{SS} = \frac{P_{in}V_s}{L} = \frac{m_{NP}W_{SLP}}{L} \tag{13}$$

where L is the overall loss factor of the system.

Such an estimate is implicitly based upon the hypothesis of a constant heating efficiency of magnetic NPs. However, when the input power is temperature dependent no simple relationship can be inferred between the final temperature and the SLP measured from the initial slope of the $\Delta T(t)$ curve, as shown in panels *(a)* and *(b)* of Figure 5, referring to NP diameters in the 10-17 nm range and to convective boundary conditions. For the reasons given in Section 2.2, the rate-equation model becomes gradually less accurate below $D = 12$ nm; therefore, the values reported in both panels should be considered as slightly less reliable, and are

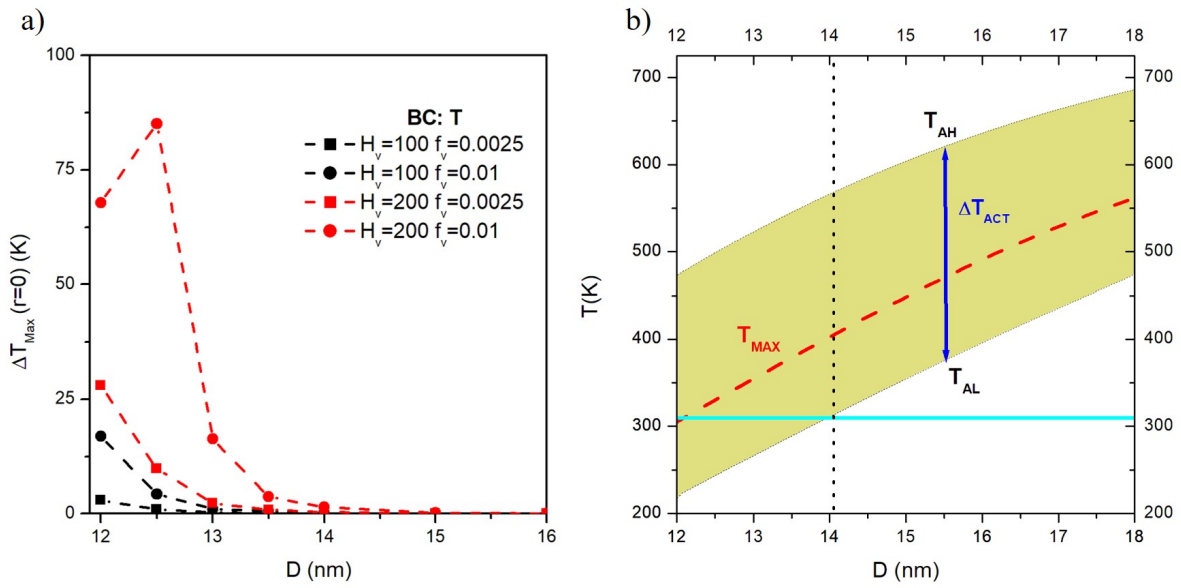

Fig. 3 a) Steady-state temperature at the center of the sample as a function of the NP diameter, for different values of vertex field H_V and particle volume fraction f_V (thermostatic BCs); b) thermal activity diagram for the considered magnetite nanopartilces. The yellow area corresponds to the region of thermal activity of nanoparticles having size between 12 and 18 nm; the horizontal line marks the starting temperature T_0 of the host medium (see text for details)

represented by open symbols. With the parameter values used in this work, a sharp maximum of the SLP occurs at $D = 12$ nm. However, the position of the peak is critically dependent on the magnetic parameters of the nanoparticles under consideration. These are in turn sensitive to many factors, including the quality of the obtained nanomaterials and the preparation technique: for instance, the value of magnetic anisotropy K_{eff} can be influenced by NP surface, whose effect depends on size and preparation technique [1]. In the experimental practice, neither the NP size nor the values of magnetic parameters are so sharply defined to ensure the absolute validity of the predictions of any theoretical model.

It is possible to evaluate ΔT_{SS} for our model system in the BC:C arrangement, applying Equation 12 and calculating the loss factor from the convective heat transfer coefficient. For a sphere of radius r one simply gets:

$$L = 4\pi b^2 h. \tag{14}$$

The result is shown in panel *(c)* of Figure 5 as a function of the W_{SLP} values reported in panel *(b)* (dashed black line). As expected, a linear relation is observed in this case between the two quantities. The actual ΔT_{SS} values obtained by solving the Fourier equation for $r \to b$ can be markedly different, and no linear relation is observed. For $D = 12$ nm, the adiabatic model predicts a temperature slightly higher than the one found in the present model; this is easily understood considering that the adiabatic model assumes a constant input power, whilst in this case P_{in} is monotonically decreasing with increasing T (see Figure 4). On the other hand, when the input power increases with increasing T and exhibits a peak, the steady-state temperatures predicted by the adiabatic model are systematically lower than the ones we obtain from the rate equations. The two models give the same final temperatures only when there is no substantial heating of the sample, i,.e., for nanoparticles with large diameters. It should be noted that the difference between the predictions of the two models does not amount to a simple offset, but is strongly dependent on the higher or lower efficiency of magnetic NPs as heating agents. This may put the standard procedure in jeopardy because it contradicts to the reliability requirement referred to in the Introduction; a way to overcome such a difficulty will be discussed in Section 4.

3.6 Tissue-blood perfusion rate in magnetic hyperthermia: a caveat

The present model allows one to recognize the importance of the convective heat flux coefficient h. Changing this parameter, in fact, brings about considerable differences in the heating efficiency of a NP system. In *in vivo* applications, the heat released by a concentration of magnetic NPs inside a small region of a living body is removed by the local tissue-blood perfusion mechanism, whose rate W is related to h by Equation 9. In the human body, the product $[Wc_b]$ is greatly dependent on type and nature of the interested tissue, typically ranging from 400-4000 W/m^{3}K in healthy tissues to 4-6$\times 10^4$ W/m^{3}K in tissues affected by tumors [73, 76, 54].

As an example of the impact of this parameter, the steady state temperature increment ΔT_{SS} in $r = b/2$ is reported in Figure 6 for values of $[Wc_b]$ roughly covering the ones actually measured in living tissues; the regions broadly corresponding to healthy and tumor-affected tissues are put in evidence in color (green / red areas, respectively). ΔT_{SS} is observed to monotonically increase

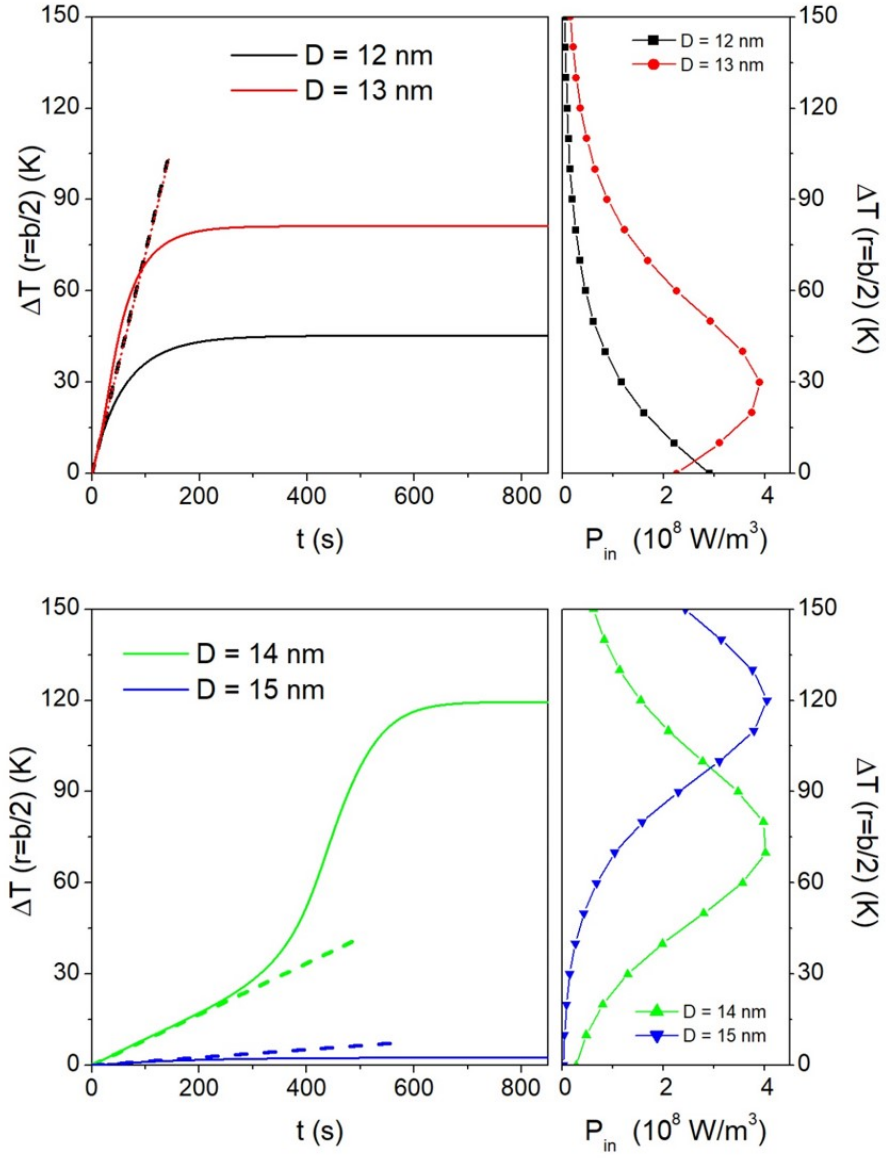

Fig. 4 Time profile of the temperature increment at $r = b/2$ and corresponding temperature behavior of the $P_{in}(T)$ curves for four NP diameters. Convective BCs. Dashed lines put in evidence the initial slope of the $T(b/2,t)$ curves.

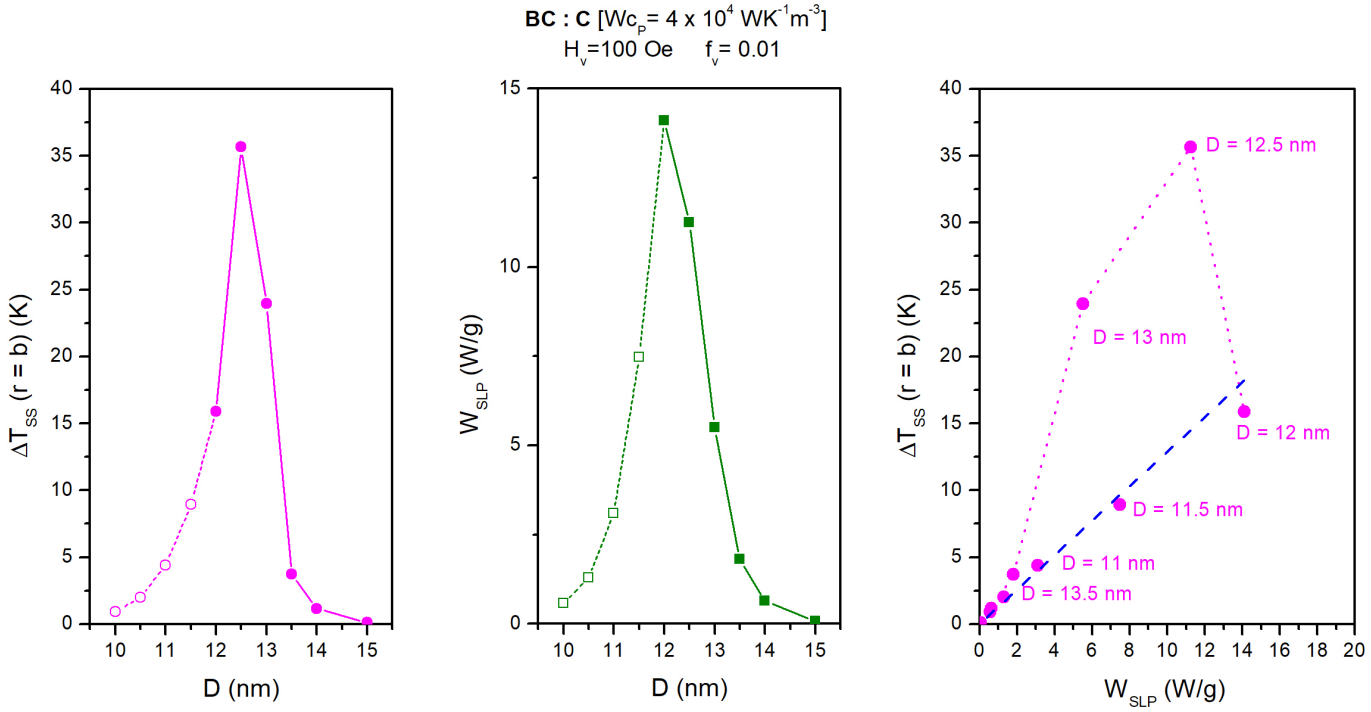

Fig. 5 *(a)* Steady-state temperature increment at the edge of the sample as a function of NP diameter, obtained from the present model in convective BCs; *(b)* specific loss power W_{SLP} evaluated according to the adiabatic model (Equations 11 and 12); *(c)* steady-state temperature increment obtained by the present model (symbols) and by the adiabatic model (dashed line) as functions of the W_{SLP} values of panel *(b)*.

with reducing $[Wc_b]$ up to values which in healthy tissues are about five times greater than the ones predicted for tissues affected by a tumor.

This result clearly indicates that the same extrinsic parameters (nanoparticle concentration, driving-field amplitude and frequency) that are beneficial in the effective treatment of a specific tumor may induce major discomfort in, or even to be dangerous to a treated patient if the nanoparticles are partially dispersed in neighboring healthy tissues also. Proper targeting of the magnetic nanoparticles is therefore an important issue, although, in view of the wide variability in the tolerance to heat usually observed in living bodies, other treatment parameters such as particle concentration at the target and method of administration play a similar, and sometimes more important role.

3.7 Nanoparticles of different size: secondary activation

A detailed study of the heating efficiency of a system of nanoparticle distributed in size is beyond the aim of this work. However, a special consequence of the temperature-dependent power needs to be emphasized. As observed in Section 3.5.1, systems of monodisperse nanoparticles whose diameters exceed some upper limit are not able to heat a host medium because the peak of the input power is displaced towards a temperature so high that it cannot be attained in the heating process. For instance, with the parameter values of Section 3.5.1, it is observed that the nanoparticles with $D = 15$ nm appear to be almost inactive. However, they can be activated in a properly prepared sample.

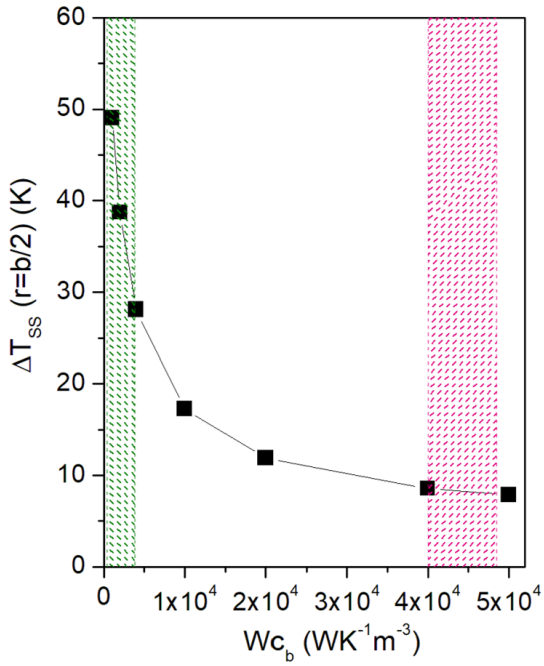

Fig. 6 Steady-state temperature predicted by the model at $r = b/2$ in convective BCs as a function of the product $[Wc_b]$ where W is the local tissue-blood perfusion rate and c_b is the blood's specific heat

Let us consider as a case study a mixture containing equal parts of magnetite particles of two sizes, D =14 nm and D =15 nm (in this case, $f_{V,14} = f_{V,15} = 0.5 f_V = 5 \times 10^{-3}$). When the alternating magnetic field is switched on, the smaller particles begin to heat the sample but the larger particles still are basically inactive. However, while the temperature gradually increases, the larger nanoparticles enter the region of the peak of $P_{in}(T)$ and begin to release appreciable amounts of magnetic power, that adds to the one from the smaller particles. Such a "secondary" activation of the larger particles leads to a further increase of the temperature. The effect is shown in Figure 7a,b where the temperature increment produced by the mixture is higher than the ones observed when the two constituents are separately considered. In actual, size-distributed NP systems, secondary activation is expected to play a non-negligible role on the temperature reached by a sample.

It should be pointed out that a significant enhancement of the target temperature (Fig. 7 b) is observed when the mixture contains a fraction of nanoparticles which are thermally inactive at the starting temperature (e.g., because they are large, as in the above discussed case). These particles can be submitted to "secondary" activation by the temperature increase resulting from other particles in the mixture, which are thermally active at the starting temperature and, in a sense, act as an initiator. On the contrary, when the mixture is comprised of multi-sized particles which are *all* thermally active since the beginning, the temperature enhancement may disappear. This is shown in Figure 7d, referring to a 50-50% mixture of nanoparticles with D =12 nm and D =13 nm in the same conditions as in the previous case. The corresponding $P_{in}(T)$ curves, reported in Fig. 7c, clearly show that both sizes provide substantial heating power since the very begining of an ideal experiment. It turns out that in this case the 50-50% mixture produces a heating curve which is intermediate between the ones obtained using monodisperse systems with D =12 nm and D = 13 nm.

4 SLP measurement: an alternative method

In Section 3.5.2 it has been shown how problematic is the estimate of the SLP when the power released by magnetic NPs depends markedly on temperature. On the other hand, experimentally determining the exact behavior of $P_{in}(T)$ for a specific NP system from magnetic measurements (i.e., from the area of hysteresis loops) is unpractical, although feasible in principle. From a fundamentalist's viewpoint, a more expedient method to determine the temperature-dependent power released by a nanoparticle system is desirable. From the viewpoint of therapeutic applications, a central question concerns how a reliable value of the SLP can be found when the adiabatic method cannot be applied.

Here, an original method of analysis of experimental $\Delta T_{exp}(t)$ curves is presented and shown to answer to both questions.

4.1 Principles of the method

Let us consider a spherical sample of radius b containing a tissue phantom loaded with a magnetite nanoparticle dispersion of volume fraction f_V, and immersed in an ice-water thermostat (Figure 8a). The temperature evolution of the sample is measured by placing two thermocouples in r =0 and in a nearby position ($r = \delta$). In practice, it is sufficient that δ be of the order of $0.1b$. Such an experimental configuration can be implemented even if b is as small as 0.01 m, as supposed here; if needed, the experimental setup is easily scalable by simultaneosuly increasing b and reducing f_V (in order to deal with the same range of steady-state temperatures considered here).

The time evolution of the incremental temperature $\Delta T_{exp}(0,t)$ and $\Delta T_{exp}(\delta,t)$ in the two positions is recorded. Using the Fourier equation, the the time evolution of the input power P_{in} in $r = 0$ is:

$$P_{in}(t) = \frac{k}{\alpha}\frac{\partial(\Delta T)}{\partial t}\Big|_{r=0} - k\Big(\frac{\partial^2(\Delta T)}{\partial r^2}\Big|_{r=0} + \Big[\frac{2}{r}\frac{\partial(\Delta T)}{\partial r}\Big]_{r=0}\Big). \quad (15)$$

On the other hand, the temperature of the sample in a point sufficiently close to $r = 0$ can always be written as:

$$\Delta T(r,t) \approx c_0(t) - c_2(t) r^2 \quad (16)$$

with time-dependent coefficients $c_{0,2}(t)$. The coefficient of the term linear in r must be zero because of the singularity of the radial Fourier equation in r =0. It should be noted that the coefficient $c_0(t)$ is equal to $\Delta T_{exp}(0,t)$. Using Equation 16 the input power is expressed as a linear combination of the derivative of the experimental heating curve in $r = 0$ and of $c_2(t)$:

$$P_{in}(t) = \frac{k}{\alpha}\frac{\partial(\Delta T)}{\partial t}\Big|_{r=0} + 6kc_2(t). \quad (17)$$

On the other hand, the coefficient $c_2(t)$ can be experimentally obained from Equation 16 by measuring the time evolution of the incremental temperature in r =0 and $r = \delta$:

$$c_2(t) = \frac{\Delta T_{exp}(0,t) - \Delta T_{exp}(\delta,t)}{\delta^2}. \quad (18)$$

Therefore, the input power in $r = 0$ is:

$$P_{in}(t) = \frac{k}{\alpha}\frac{\partial(\Delta T_{exp})}{\partial t}\Big|_{r=0} + \frac{6k}{\delta^2}\big(\Delta T_{exp}(0,t) - \Delta T_{exp}(\delta,t)\big). \quad (19)$$

All functions appearing in the right-hand side of Equation 19 are either experimental data or quantities easily obtained by simple post-processing of experimental data.

4.2 Evaluating the temperature-dependent released power $P_{in}(T)$ from $\Delta T_{exp}(t)$ curves

The behavior of P_{in} as a function of time in $r = 0$ can be immediately associated to the evolution of incremental temperature in the same point, $\Delta T_{exp}(0,t)$. In this way the temperature dependence of P_{in} is obtained. The self-consistency of the approach has been checked: the dotted curves in Figure 8b represent the input power obtained from the hysteresis loops for three nanoparticle diameters, whereas the lines represent the input power obtained by analysing the resulting $\Delta T_{exp}(0,t)$ and $\Delta T_{exp}(\delta,t)$ curves by means of Equation 19. The $P_{in}(t \to T)$ values obtained in this way are perfectly superimposed to the corresponding starting curves.

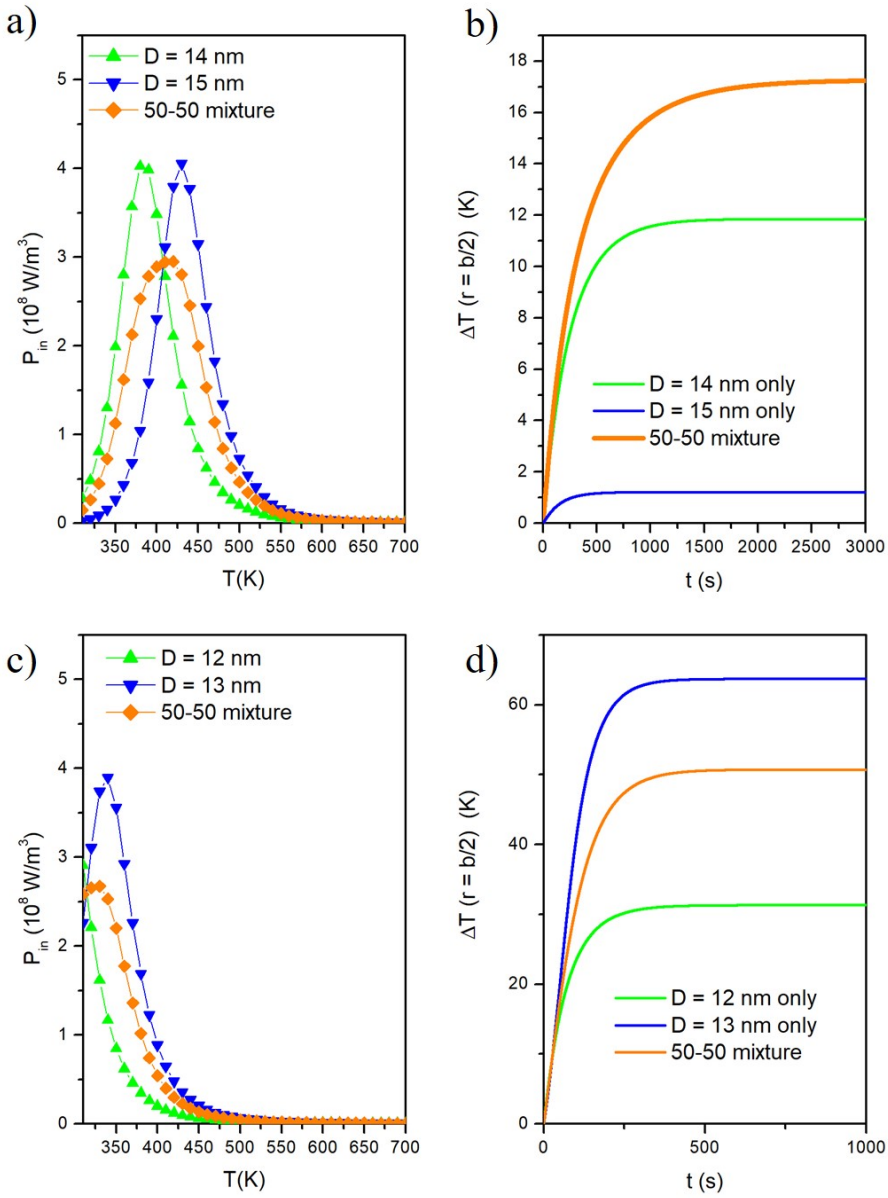

Fig. 7 *(a)* Temperature-dependent input power for $H_V = 200$ Oe and monodisperse NPs with D =14, 15 nm and for a 50-50 mixture of the two diameters; *(b)* corresponding time profiles of the temperature increment in $r = b/2$; *(c, d)* The same for monodisperse NPs with D =12, 13 nm and for a 50-50 mixture of the two diameters.

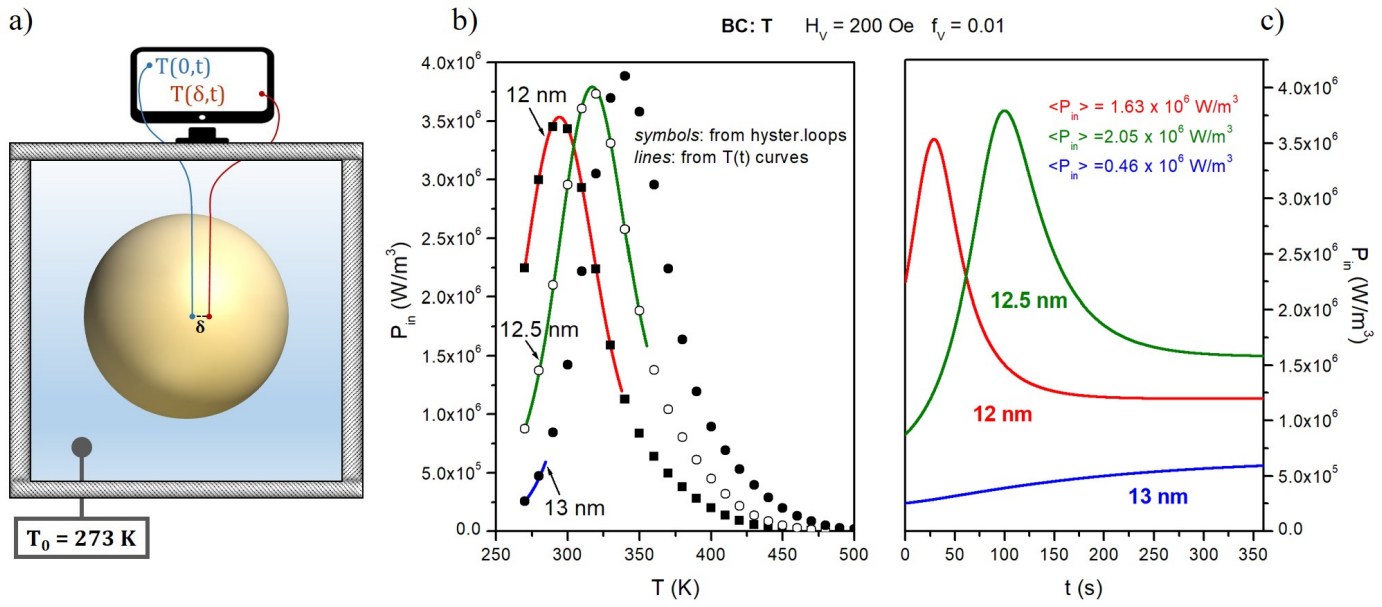

Fig. 8 *(a)* Sketch of the measurement setup with sample kept inside an ice-water thermostat; *(b)* symbols: $P_{in}(T)$ data obtained from hysteresis loops; lines: the same quantities obtained by the proposed measurement method (Equation 19) for three NP diameters; *(c)* instantaneous input power in $r=0$ for the same diameters; time averaged values of P_{in} are also given.

Of course, this method does not allow one to obtain the full $P_{in}(T)$ curve, but only a part of it, i.e., the one between T_0 and $T_{SS}=T_0+\Delta T_{exp}(0,\infty)$. The lower the final temperature reached by the sample, the narrower the investigated region of $P_{in}(T)$. The effect strongly depends on NP diameter, as clearly shown by the three curves in Figure 8b.

In this way, the heating power of magnetic nanoparticles is experimentally determined from temperature measurements without the need of measuring magnetic properties.

4.3 Evaluating the average SLP in a heating experiment

The time dependence of the input power in the heating process is reported in Figure 8c for three different NP sizes. The instantaneous power turns out to markedly vary during the heating process, and can exhbit a sharp maximum. It is possible to check that the $P_{in}(t)$ curve is extremely sensitive, in both amplitude and shape, to the NP diameter, a small change of D resulting in a great change of P_{in}. The present results show that trying to characterize the heating efficiency of a specific NP system by a single parameter (e.g., the SLP) can be useless when the temperature dependence of the input power plays a major role. In fact, the overall heating efficiency depends on both the instantaneous input power and the time elapsed since the start of the heating treatment. If one looks for a single parameter representing the power actually released by magnetic nanoparticles, the average of P_{in} over a given time interval can be used. The values of $<P_{in}>$ evaluated for the three NP diameters over the time interval shown in Figure 8c are also reported. Putting these values in Equation 11 gives a more reliable estimate of the specific loss power W_{SLP} than the adiabatic method. The results are summarized in Table 1 along with the final temperatures $T_{SS}(r=0)$. The prediction of the adiabatic method (Equation 12) is largely inaccurate, reflecting the initial behavior of the heating curve that is not simply related to the the overall time development of $T(t)$ during the treatment. It should be noted that the analysis of the initial part of the $T(t)$ curve either overestimates or underestimates the SLP evaluated by the present method. Instead, the W_{SLP} values obtained from $<P_{in}>$ and including all the features of the $T(t)$ curve are roughly proportional to the final temperatures. The data of Table I show that a good heating performance can be achieved over an appreciable range of particle diameters.

These results imply that it is not possible to define a *single* parameter that can be confidently used as a unambiguous label of the heating efficiency of a specific NP powder. Actually, even the W_{SLP} value obtained through the average power $<P_{in}>$ cannot be considered as a single parameter, because it depends on the time interval used for taking the average.

5 Conclusions

The rate equation model has been applied to assess the temperature dependence of the power released by systems of noninteracting, monodisperse magnetite nanoparticles, as well as the consequences on their efficiency as heating elements under an alternating driving field. The tunable parameters used in this work (vertex field, driving-field frequency, nanoparticle volume concentration) are compatible with the present-day therapeutic practice. The main results of our approach are:

- the area of the hysteresis loops has been shown to be a non-monotonic function of temperature, so that the power P_{in} released by the NPs presents a peak whose position in temperature depends on NP size; a heuristic explanation of this dependence has

Table 1 Comparison between SLP values obtained in adiabatic conditions and from the present model for three NP diameters. The steady-state temperature in the middle of the sample is also reported.

D (nm)	10	10.5	11	11.5	12	12.5	13	13.5	14	15
W_{SLP} (W/g) *	6.27	15.75	37.79	65.58	48.97	17.96	5.06	1.91	0.81	0.08
W_{SLP} (W/g) †	**4.89**	**9.75**	**16.67**	**24.58**	**31.62**	**39.77**	**8.92**	**2.16**	**0.85**	**0.08**
$T_{SS}(r=0)$ (°C)	8.63	17.77	32.18	50.49	67.84	85.09	16.33	3.69	1.46	0.15

* Adiabatic conditions, Equation 12
† Present work, Equation 19

been given;
- the effect of the temperature-dependent input power on the heating efficiency of NPs homogeneously distributed inside a spherical sample has been studied by solving the Fourier equation with two typical boundary conditions; in particular, the convective BC simulates the heating behavior of a portion of living tissue populated by magnetic NPs and exchanging heat with the environment through the blood flux, likening the model to the bioheat equations;
- the linear loss model, where the input power is derived from the imaginary part of the complex magnetic susceptibility, gives incorrect results when the vertex field takes values like the ones used in the therapeutic practice;
- the solutions of the heat transport equation show that:

a) the heating efficiency of magnetic NPs is high in a very narrow range of diameters; particles with diameters outside such a region (a few nanometers wide) are basically inactive; a thermal activity diagram helps to predict the optimal thermal efficiency of a NP system;
b) the time evolution of the temperature increment of the medium can be complex: the shape of the profile strongly depends on NP size and is unpredictable from the measurement of $T(t)$ during the first stages of heating; the same comment applies to the final (steady-state) temperature;
c) secondary activation of initially inactive NPs can occur in mixtures containing particles of different size;

-therefore, determining the specific loss power of a NP system by measurements of the initial slope of the $T(t)$ curve in adiabatic conditions gives incorrect results when the input power is dependent on temperature; the final temperature of a sample is generally not linked by a simple expression to the SLP determined in the adiabatic-measurement framework;
- the functional dependence on temperature of the magnetic quantities should not be neglected even if the host medium's temperature is changed by a few degrees only;
- in convective BCs, the convective heat transfer coefficient plays a central role on the steady-state temperature of a sample; in living bodies, such a quantity is directly proportional to the tissue-blood perfusion rate W that varies by orders of magnitude between healthy and malignant tissues; in the therapeutic practice, great attention is to be paid to ensure proper targeting of the NPs on malignant tissues without affecting neighboring healthy tissues.

Finally, we have proposed a simple experimental method to determine both the temperature dependence of the input power P_{in} without making use of magnetic measurements, and the instantaneous power relased by NPs during the heating process. The method is based on measurement and analysis of the time evolution of temperature. From the knowledge of the instantaneous power it is then possible to derive the average power actually released by the magnetic NPs to an host medium and a more correct value of the specific loss power.

Of course, optimizing the thermal efficiency of a NP system is just *one* of the requirements for therapeutic effectiveness of magnetic hyperthermia. In particular, the success of *in vivo* precision nanomedicine is related to correct vehiculation and targeting of the heating particles [81, 82] and to the ability of the healing agents to penetrate in depth in the malignant tissue[25, 26]. Magnetic nanoparticles have the advantage of bringing the heat source deeply within a tumor, which enhances their healing effect, overcoming the problems inherent to thermotherapies whose heat source is placed externally. Even in the case of magnetic hyperthermia, a further improvement will possibly arise by proper combination of thermotherapy and chemotherapy [65]. Moreover, driving magnetic nanoparticles by means of tailored field gradients can add a degree of freedom helping research groups to optimize the drug targeting performance, which is one of the key factors for the efficiency of this type of precision nanomedicine [26].

Finally, the present deficiencies of magnetic nanoparticles for hyperthermia and the possible strategies to increase a reliable use in the therapeutic practice are briefly discussed. As recently pointed out [65], the present limiting factors include the difficulty to compare results from different research groups and the absence of definite experimental protocols. This paper may help solving the latter problem, because it suggests a way to standardize the devices designed for SLP measurement. Another problem arises from the present lack of uniformity of the measurement practices in *in vivo* treatments, which can lead to inconclusive results because of the use of inadequate animal models [65]. Other strategic improvements involve the accurate NP localization in the living body and the measurement of the local temperature actually reached by the target. In our view, however, all future improvements in the therapeutic practice need to be firmly based upon the precise knowledge of the thermal performance of magnetic nanoparticles. It is believed that this paper is a step forward in this direction.

6 Supplementary Material

Supplementary Material (available online) includes analytic details about the rate equations applied to magnetic DWS, including the different forms taken using either time or magnetic field as independent variable. The steps leading to the expression of the cyclic magnetization are summarized. A brief discussion of the validity conditions of the rate-equation approach in treating magnetization dynamics is also provided.

Notes and references

7 References

1 S. P. Gubin, *Magnetic Nanoparticles* (Wiley, 2009).

2 V. Chaudhary, R. Chaudhary, Magnetic Nanoparticles:Synthesis, Functionalization, and Applications in *Enciclopedia of Nanoscience and Nanotechnology*, Vol. 29, 153-183 (2018).

3 W. Yang, W. Lei, Y. Yu, W. Zhu, T. A. George, X.-Z. Li,D. J. Sellmyer, S. Sun, From FePt– Fe_3O_4 to $L1_0$-FePt–Fe nanocomposite magnets with a gradient interface. *J. Mater. Chem. C*, **3**, 7075–7080 (2015).

4 U. Wiedwald, P. Ziemann, *Properties and applications of magnetic nanoparticles* (Beilstein Journal of Nanotechnology, 2019).

5 W. Lei, Y. Yu, W. Yang, M. Feng, H. Li, A general strategy for synthesizing high-coercivity $L1_0$-FePt nanoparticles. *Nanoscale*, **9**, 12855–12861 (2017).

6 W. Lei, J. Xu, Y. Yu, W. Yang, Y. Hou, D. Chen, Halide Ion-Mediated Synthesis of $L1_0$-FePt Nanoparticles with Tunable Magnetic Properties. *Nano Lett.*, **18**, 7839–7844 (2018).

7 W. Lei, Y. Yu, W. Yang, Cu induced low temperature ordering of fct-FePtCu nanoparticles prepared by solution phase synthesis. *J. Mater. Chem. C*, **7**, 11632–11638 (2019).

8 G. Han, Y. Liu, W. Yang, S. Geng, W. Cui, Y. Yu, Fabrication, characterization, and magnetic properties of exchange-coupled porous $BaFe_8Al_4O_{19}/Co_{0.6}Zn_{0.4}Fe_2O_4$ nanocomposite magnets. *Nanoscale*, **11**, 10629–10635 (2019).

9 D. Makarov, M. Melzer, D. Karnaushenko, O. G. Schmidt, Shapeable magnetoelectronics. *Appl. Phys. Rev.* **3**, 011101 (2016).

10 C. Binns, *Nanomagnetism: Fundamentals and Applications* (Elsevier, 2014).

11 Z. Wu, T. Li, J. Li, W. Gao T. Xu, C. Christianson W. Gao, M. Galarnyk, Q. He, L. Zhang, J. Wang, Turning erythrocytes into functional micromotors. *Acs Nano* **8** , 12041–12048 (2014).

12 L. Mohammed, H. G. Gomaa, D. Ragab, J. Zhu, Magnetic nanoparticles for environmental and biomedical applications: A review. *Particuology*, **30** , 1–14 (2017).

13 S. Lantean, G. Barrera, C. F. Pirri, P. Tiberto, M. Sangermano, I. Roppolo, G. Rizza, 3D Printing of Magnetoresponsive Polymeric Materials with Tunable Mechanical and Magnetic Properties by Digital Light Processing. *Adv. Mater. Technol.*, 1900505 (2019).

14 P. Allia, G. Barrera, P. Tiberto, Nonharmonic Driving Fields for Enhancement of Nanoparticle Heating Efficiency in Magnetic Hyperthermia, *Phys. Rev. Appl.*,**12**, 034041, (2019).

15 N. T. K. Thanh, *Clinical applications of magnetic nanoparticles* (CRC Press, 2018).

16 A. N. Khan, A. Ermakov, G. Sukhorukov, Y. Hao, Radio frequency controlled wireless drug delivery devices. *Appl. Phys. Rev.*, **6** , 041301 (2019).

17 N. D. Thorat, S. A. M. Tofail, B. von Rechenberg, H. Townley, G. Brennan, C. Silien, H. M. Yadav, T. Steffen, J. Bauer, Physically stimulated nanotheranostics for next generation cancer therapy: Focus on magnetic and light stimulations. *Appl. Phys. Rev.*, **6** , 041306 (2019).

18 X. Li Liu, E. S. G. Choo, A. S. Ahmed, L. Y. Zhao, Y. Yang, R. V. Ramanujan, J. M. Xue, D. D. Fan, H. M. Fan, J. Ding, Magnetic nanoparticle-loaded polymer nanospheres as magnetic hyperthermia agents. *J. Mater. Chem. B*, **1**, 120–128 (2014).

19 X. L. Liu, Y. Yang, C. T. Ng, L. Y. Zhao, Y. Zhang, B. H. Bay, Hai Ming Fan, Jun Ding, Magnetic Vortex Nanorings: A New Class of Hyperthermia Agent for Highly Efficient In Vivo Regression of Tumors. *Adv Mater.*, **27**, 1939–1944 (2015).

20 L. Zhu, Z. Zhou, H. Mao, L. Yang, Magnetic nanoparticles for precision oncology: Theranostic magnetic iron oxide nanoparticles for image-guided and targeted cancer therapy. *Nanomedicine*, **12** , 73–87 (2017)

21 S. D. Jo, S. H. Ku, Y-Y Won, S. H. Kim, I. C. Kwon, Targeted nanotheranostics for future personalized medicine: Recent progress in cancer therapy. *Theranostics*, **6** , 1362–1377 (2016).

22 M. Hu, X. Ai, Z. Wang, Z. Zhang, H., Cheong, W. Zhang, J. Lin, J. Li, H. Yang, B. Xing, Nanoformulation of metal complexes: Intelligent stimuli-responsive platforms for precision therapeutics. *Nano Res.*, **11**, 5474–5498 (2018).

23 Y. Qiao, J. Wan, L., Zhou, W. Ma, Y. Yang, W. Luo, Z. Yu, H. Wang, Stimuli-responsive nanotherapeutics for precision drug delivery and cancer therapy. *WIRES Nanomed. Nanobi.*, **11** , 1–20 (2018).

24 E. A. Périgo, G. Hemery, O. Sandre, D. Ortega, E. Garaio, F. Plazaola, F. J. Teran, Fundamentals and advances in magnetic hyperthermia. *Appl. Phys. Rev.*, **2** , 041302 (2015).

25 Y. Zhang, R. Sha, L. Zhang, W. Zhang, P. Jin, W. Xu, J. Ding, J. Lin, J. Qian, G. Yao, R. Zhang, F. Luo, J. Zeng, J. Cao, L. Wen, Harnessing copper-palladium alloy tetrapod

nanoparticle-induced pro-survival autophagy for optimized photothermal therapy of drug-resistant cancer. *Nat. Commun.*, **9** , 4236 (2018).

26 J. Ding, J. Chen, L. Gao, Z. Jiang, Y. Zhang, M. Li, Q. Xiao, S. S. Lee, X. Chen, Engineered nanomedicines with enhanced tumor penetration. *Nano Today*, **29**, 100800 (2019).

27 B. T. Mai, S. Fernandes, P. B. Balakrishnan, T. Pellegrino, Nanosystems Based on Magnetic Nanoparticles and Thermo- or pH-Responsive Polymers: An Update and Future Perspectives. *Acc. Chem. Res.*, **51** , 999–1013 (2018).

28 I. Ortiz de Solorzano, T. Alejo, M. Abad, C. Bueno-Alejo, G. Mendoza, V. Andreu, s., Irusta, V. Sebastian, M. Arruebo, Cleavable and thermo-responsive hybrid nanoparticles for on-demand drug delivery. *J. Colloid Interf. Sci.*, **533** pp. 171–181 (2019).

29 K. Maier-Hauff, F. Ulrich, D. Nestler, H. Niehoff, P. Wust, B. Thiesen, H. Orawa, V. Budach, A. Jordan, Efficacy and safety of intratumoral thermotherapy using magnetic iron-oxide nanoparticles combined with external beam radiotherapy on patients with recurrent glioblastoma multiforme. *J. Neurooncol.*, **103** , 317–324 (2011).

30 web site: https://magforce.com/en/home/our_therapy/

31 S. Dutz, R. Hergt, Magnetic nanoparticle heating and heat transfer on a microscale: Basic principles, realities and physical limitations of hyperthermia for tumour therapy. *Int. J. Hyperthermia*, **29** , 790–800 (2013).

32 P. J. Vikesland, R. L. Rebodos, J. Y. Bottero, J. Rose, A. Masion, Aggregation and sedimentation of magnetite nanoparticle clusters. *Environ. Sci. Nano*, **3**, 567–577 (2016).

33 P. Tartaj, S. Veintemillas-Verdaguer, T. Gonzalez-Carreño, C. J. Serna, Preparation of Magnetic Nanoparticles for Applications in Biomedicine in *Magnetic Nanoparticles in Biosensing and Medicine* 52–67, (Cambridge University Press, 2019).

34 L. C. Branquinho, M. S. Carrião, A. S. Costa, N. Zufelato, M. H. Sousa, R. Miotto, R. Ivkov, A. F. Bakuzis, Effect of magnetic dipolar interactions on nanoparticle heating efficiency: Implications for cancer hyperthermia *Sci. Rep.*, **3** pp. 20–22 (2013).

35 D. F. Coral, P. M. Zélis, M. Marciello, M. del Puerto Morales, A. Craievich, F. H. Sánchez, M. B. Fernández van Raap, Effect of Nanoclustering and Dipolar Interactions in Heat Generation for Magnetic Hyperthermia. *Langmuir*, **32** , 1201–1213 (2016).

36 C. Guibert, V. Dupuis, V. Peyre, J. Fresnais, Hyperthermia of Magnetic Nanoparticles: Experimental Study of the Role of Aggregation. *J. Phys. Chem. C*, **119** , 28148–28154 (2015).

37 C. Martinez-Boubeta, K. Simeonidis, D. Serantes, I. Conde-Leborán, I. Kazakis, G. Stefanou, L. Peña, R. Galceran, L. Balcells, C. Monty, D. Baldomir, M. Mitrakas, M. Angelakeris, Adjustable hyperthermia response of self-assembled ferromagnetic Fe-MgO core-shell nanoparticles by tuning dipole-dipole interactions. *Adv. Funct. Mater.*, **22**, 3737–3744 (2012).

38 D. Serantes, D. Baldomir, C. Martinez-boubeta, K. Simeonidis, M. Angelakeris, E. Natividad, M. Castro, A. Mediano, D.-X. Chen, A. Sanchez, L. Balcells, B. Martínez, Influence of dipolar interactions on hyperthermia properties of ferromagnetic particles. *J. Appl. Phys.*, **108**, 073918 (2010).

39 R. R. Wildeboer, P. Southern, Q. A. Pankhurst, On the reliable measurement of specific absorption rates and intrinsic loss parameters in magnetic hyperthermia materials. *J. Phys. D: Appl. Phys.*, **47**, 495003 (2014).

40 L. Del Bianco, F. Spizzo, G. Barucca, M. R. Ruggiero, S. Geninatti Crich, M. Forzan, E. Sieni, P. Sgarbossa, Mechanism of magnetic heating in Mn-doped magnetite nanoparticles and the role of intertwined structural and magnetic properties. *Nanoscale*, **11** , 10896–10910 (2019).

41 R. E. Rosenweig, Heating magnetic fluid with alternating magnetic field. *J. Magn. Magn. Mater.*, **252** , 370–374 (2002).

42 E. Garaio, O. Sandre, J-M. Collantes, J. A. Garcia, S. Mornet, F. Plazaola, Specific absorption rate dependence on temperature in magnetic field hyperthermia measured by dynamic hysteresis losses (ac magnetometry). *Nanotechnology*, **26** , 015704 (2015).

43 M. Coïsson, G. Barrera, F. Celegato, L. Martino, S. N. Kane, S. Raghuvanshi, F. Vinai, P. Tiberto, Hysteresis losses and specific absorption rate measurements in magnetic nanoparticles for hyperthermia applications. *BBA-Gen Subjects*, **1861** , 1545–1558 (2017).

44 E. Natividad, M. Castro, A. Mediano, Adiabatic magnetothermia makes possible the study of the temperature dependence of the heat dissipated by magnetic nanoparticles under alternating magnetic fields. *Appl. Phys. Lett.*, **98**, 243119 (2011).

45 M. Beković, M. Trlep, M. Jesenik, V. Goričan, A. Hamler, An experimental study of magnetic-field and temperature dependence on magnetic fluid's heating power. *J. Magn. Magn. Mater.*, **331** pp. 264–268 (2013).

46 S. Dutz, R. Hergt, Magnetic particle hyperthermia - A promising tumour therapy? *Nanotechnology*. **25** , 452001 (2014).

47 R. Di Corato, A. Espinosa, L. Lartigue, M. Tharaud, S. Chat, T. Pellegrino, C. Ménager, F. Gazeau, C. Wilhelm, Magnetic hyperthermia efficiency in the cellular environment for different nanoparticle designs. *Biomaterials*, **35**, 6400–6411 (2014).

48 D. Soukup, S. Moise, E. Céspedes, J. Dobson, N. D. Telling, In Situ Measurement of Magnetization Relaxation of Internalized Nanoparticles in Live Cells. *ACS Nano*, **8**, 231-240 (2015).

49 N. A. Usov, Numerical simulation of field-cooled and zero field-cooled processes for assembly of superparamagnetic nanoparticles with uniaxial anisotropy. *J. Appl. Phys.*, **109** 023913 (2011).

50 J. Carrey, B. Mehdaoui and M. Respaud, Simple models for dynamic hysteresis loop calculations of magnetic single-domain nanoparticles: Application to magnetic hyperthermia optimization, J. Appl. Phys. **109**, 083921 (2011)

51 P. Allia, G. Barrera and P. Tiberto, Linearized rate-equation approach for double-well systems: Cooling- and temperature-dependent low-field magnetization of magnetic nanoparticles, Phys. Rev. B **98**, 134423 (2018).

52 P. Allia, G. Barrera, P. Tiberto, Hysteresis effects in magnetic nanoparticles: A simplified rate-equation approach. *J. Magn. Magn. Mater.*, **496**, 165927, (2020).

53 C. L. Ondeck, A. H. Habib, P. Ohodnicki, K. Miller, C. A. Sawyer, P. Chaudhary, M. Mchenry, Theory of magnetic fluid heating with an alternating magnetic field with temperature dependent materials properties for self-regulated heating. *J. Appl. Phys.*. **105** , 103–106 (2009).

54 M. Ebrahimi, On the temperature control in self-controlling hyperthermia therapy. *J. Magn. Magn. Mater.*, **416**, 134–140 (2016).

55 I. M. Obaidat, B. Issa, Y. Haik, Magnetic Properties of Magnetic Nanoparticles for Efficient Hyperthermia. *Nanomaterials*, **5**, 63–89 (2015).

56 D. J. Dunlop, Fundamentals of Magnetism, in *Rock Magnetism* (Cambridge University Press, 1997).

57 D. J. Dunlop, Superparamagnetic and Single-Domain Threshold Sizes in Magnetite. *J. Geophys. Res.*, **78**, 1780–1793 (1973).

58 Y. V. Kolenko, M. Banobre-López, C. Rodríguez-Abreu, E. Carbó-Argibay, F. L. Deepak, D. Y. Petrovykh, M. Fátima Cerqueira, S. Kamali, K. Kovnir, D. V. Shtansky, O. I. Lebedev, J. Rivas, High-Temperature Magnetism as a Probe for Structural and Compositional Uniformity in Ligand-Capped Magnetite Nanoparticles. *J. Phys. Chem. C*, **118**, 28322–28329 (2014).

59 J. Wang, H. Duan, X. Lin, V. Aguilar, A. Mosqueda, G-m. Zhao, Temperature dependence of magnetic anisotropy constant in iron chalcogenide Fe_3Se_4: Excellent agreement with theories. *J. Appl. Phys.*, **112**, 103905 (2012).

60 D. O. Smith, Magnetization of a Magnetite Single Crystal Near the Curie Point. *Phys. Rev.*, **102**, 959–963 (1956).

61 J. Wang, W. Wu, F. Zhao, G-m. Zhao, Curie temperature reduction in SiO_2 -coated ultrafine Fe_3O_4 nanoparticles: Quantitative agreement with a finite-size scaling law. *Appl. Phys. Lett.*, **98** , 083107 (2011).

62 W. F. Brown jr., Thermal fluctuations of a single-domain particle. *Phys. Rev.*, **130** , 1677–1686 (1963).

63 N. T. K. Thanh, *Magnetic Nanoparticles from Fabrication to Clinical Applicatons* (CRC Press, 2012).

64 S. L. Berry, K. Walker, C. Hoskins, N. D. Telling, H. Price, Nanoparticle-mediated magnetic hyperthermia is an effective method for killing the human-infective protozoan parasite Leishmania mexicana in vitro. *Sci. Rep.*, **9** , 1–9 (2019).

65 L. Beola, L. Gutiérrez, V. Grazú, and L. Asín A Roadmap to the Standardization of In Vivo Magnetic Hyperthermia in *Nanomaterials for Magnetic and Optical Hyperthermia Applications* edited by R. M. Fratila and J. M. De La Fuente (Elsevier, 2019) and references therein.

66 W. J. Atkinson, I. A. Brezovich and D. P. Chakraborty, Usable Frequencies in Hyperthernia with Thermal Seeds. *IEEE Trans. Biomed. Engin.*, **31**, 70–75, (1984).

67 H-W. Huang, T-L. Horng, Bioheat transfer and Thermal Heating for tumor treatment in *Heat Transfer and Fluid Flow in Biological Processes* (Elsevier, 2015).

68 Y. Tang, R. C. C. Flesch, T. Jin, Numerical analysis of temperature field improvement with nanoparticles designed to achieve critical power dissipation in magnetic hyperthermia. *J. Appl. Phys.*, **122** 034702 (2017).

69 Y. Yuan, C. Wyatt, P. Maccarini, P. Stauffer, O. Craciunescu, J. Macfall, M. Dewhirst, S. K. Das, A heterogeneous human tissue mimicking phantom for RF heating and MRI thermal monitoring verification. *Phys Med Biol.*, **57** 2021–2037 (2012).

70 R. O. A. Jaime, R. L. Q. Basto, B. Lamien, E. R. B. Orlande. S. Eibner, O. Fudym, Fabrication methods of phantoms simulating optical and thermal properties. *Procedia Engineering*, **59** pp. 30–36 (2013).

71 For instance, it is easily shown that a single magnetite NP with a diameter of 15 nm is not able to appreciably increase the temperature of a thermostated sphere of water having a radius of 60 nm (corresponding to a volume fraction of magnetite f_V of about 1%), even if a power as high as 1×10^8 W/m^3 is released by the particle (see Figure 1c). Actually, the model predicts that in the steady state the innermost layers of the water sphere (i.e., those closest to the nanoparticle surface) are appreciably heated; however, the temperature drops very rapidly (i.e., on the nanometer scale) with increasing distance from the NP surface, so that the mean increment of water temperature remains close to zero.

72 J. Lang, B. Erdmann, M. Seebass, Impact of nonlinear heat transfer on temperature control in regional hyperthermia. *IEEE Trans. Biomed. Engin.*, **46** , 1129–1138 (1999).

73 E. Y-K. Ng, N. M. Sudharsan, Computer simulation in conjunction with medical thermography as an adjunct tool for early detection of breast cancer, *BMC Cancer*, **4** , 1–6 (2004).

74 T-C. Shih, P. Yuan, W-L. Lin, H-S. Kou, H. Analytical analysis of the Pennes bioheat transfer equation with sinusoidal heat flux condition on skin surface. *Med. Eng. Phys.*. **29** , 946–953 (2007).

75 M. L. Van Der Gaag, M. De Bruijne, T. Samaras, J Van Der Zee, G. C. Van Rhoon, Development of a guideline for the water bolus temperature in superficial hyperthermia. *Int. J. Hyperthermia*, **22** , 637–656 (2006).

76 A. Chanmugam, R. Hatwar, C. Herman, Thermal analysis of cancerous breast model. *Int. Mech. Eng. Congress Expo. 2012*, 134–143 (2012).

77 A. R. Melo, M. M. S. Loureiro, F. Loureiro, Blood Perfusion Parameter Estimation in Tumors by means of a Genetic Algorithm. *Procedia Computer Science*. **108** pp. 1384–1393 (2017).

78 Q. A. Pankhurst, N. K. T. Thanh, S. K. Jones, J. Dobson, Progress in applications of magnetic nanoparticles in biomedicine. *J. Phys. D: Appl. Phys.*, **42**, 224001 (2009)

79 S. Kossatz, R. Ludwig, H. Dähring, V. Ettelt, G. Rimkus,M. Marciello, G. Salas, V. Patel, F. J. Teran, I. Hilger, High therapeutic efficiency of magnetic hyperthermia in xenograft models achieved with moderate temperature dosages in the tumor area. *Pharm. Res.*. **31** , 3274–3288 (2014).

80 D. W. Hahn, M. N. Özisik Heat conduction (Wiley, 2012).

81 E. A. Sykes, J. Chen, G. Zheng, W. C. W. Chan, Investigating the Impact of Nanoparticle Size on Active and Passive Tumor Targeting Efficiency. *ACSnano*. **8** , 5696–5706 (2014).

82 S. Wilhelm, A. J. Tavares, Q. Dai, S. Ohta, J. Audet, H. F. Dvorak, W. C. W. Chan, Analysis of nanoparticle delivery to tumours. *Nat. Rev. Mater.*. **1**, 16014 (2016).

A Comparison between the power calculated from rate equations and the linear expression

The expression of the power released by nanoparticles submitted to an alternating field (Equation 5) was developed in the linear Debye-relaxation framework; the implicit assumption of the model is that the effect of a driving field can be viewed as a weak perturbation of the equilibrium state of the system. The formula for P_{LIN} has been and is widely applied in the area of magnetic heating of living tissues, without however considering that the driving fields most commonly used in practical applications [65] (100-250 Oe, i.e. 9-20 kA/m) typically exceed the limits of validity of the linear theory. In fact, for vertex field values such as the ones considered in our paper (100 - 200 Oe) the magnetic response of the system is no longer linear, as clearly shown by the rate equation approach [52, 14].

The loops calculated by the rate equations at H_V =100 Oe, $f = 1 \times 10^5$ Hz for T =300 K and 350 K are shown in the left panel of Figure 9 (full lines). The loops obtained in the Debye-relaxation framework [41] in the same conditions are also reported (dashed lines); they considerably differ, in shape, inclination and enclosed area, from the exact curves. As a consequence, the power vs. temperature curves predicted by the linear expression, although displaying features similar to the ones of the more accurate model, fail to account for magnitude and position of the peak of $P_{in}(T)$, as shown in the right panel of Figure 9.

B Temperature-dependent vs. constant input power for low temperature increments

Aim of this section is to study the effect of a temperature-dependent input power in heating treatments where the desired increment of temperature of the medium (e.g., a malignant tissue) with respect to the initial temperature is typically very low and must be kept as controlled as possible. The convective spherical model is used, with $f_V = 0.0025$ and H_V =100 Oe. The product $[Wc_b]$ has the value 4×10^4 W/m^{3}s typical of malignant tissues. The steady state temperatures and the time evolution profiles at $r = b/2$ obtained solving the Fourier equation with convective BCs and with the temperature-dependent input power of Figure 1c are shown in Figure 10 for two NP diameters (full lines). In these conditions, the temperature increment never exceeds 12 K.
The Fourier equaition is solved for comparison using a constant input power, with the value of P_{in} derived from the hysteresis loop at T_0 =310 K. In this case, the Fourier equation in radial symmetry admits analytical solutions. The steady-state temperature profile is given by:

$$\Delta T_{SS}(r,\infty) = \frac{P_{in}\, b}{3h} + \frac{P_{in}}{6k}(b^2 - r^2) \tag{20}$$

where h is given by Equation 9 and k is the thermal conductivity of the medium. The time profile of the temperature increment is:

$$\Delta T(r,t) = \frac{P_{in}\, b}{3h} + \frac{P_{in}}{6k}(b^2 - r^2) + \sum_{n=1}^{\infty} C_n \frac{sin\lambda_n r}{r} e^{-\alpha\lambda_n^2 t} \tag{21}$$

where α is the thermal diffusivity and the sets of constants C_n and λ_n are obtained solving suitable transcendental or integral equations [80]. The solutions of Equations 20 and 21 are reported in Figure 10 (dashed lines). For all diameters, relative differences of more than 15 % between the two sets of curves are observed. The curves do not differ by a mere shift: it is the shape of the temperature profile that changes. For $D = 12$ nm the steady-state profile obtained with temperature-dependent input power is lower than the one at constant P_{in}, while the opposite occurs for $D = 13$ nm. This effect is easily understood considering that for $D = 12$ nm the temperature-dependent $P_{in}(T)$ monotonically decreases with increasing temperature with respect to the value at $T = T_0$, while for $D = 13$ nm the same quantity exhibits the opposite behavior (see Figure 4). Therefore, keeping constant the input power can either overestimate or underestimate the actual temperature increment.

The present example shows that even in the case of small tem-

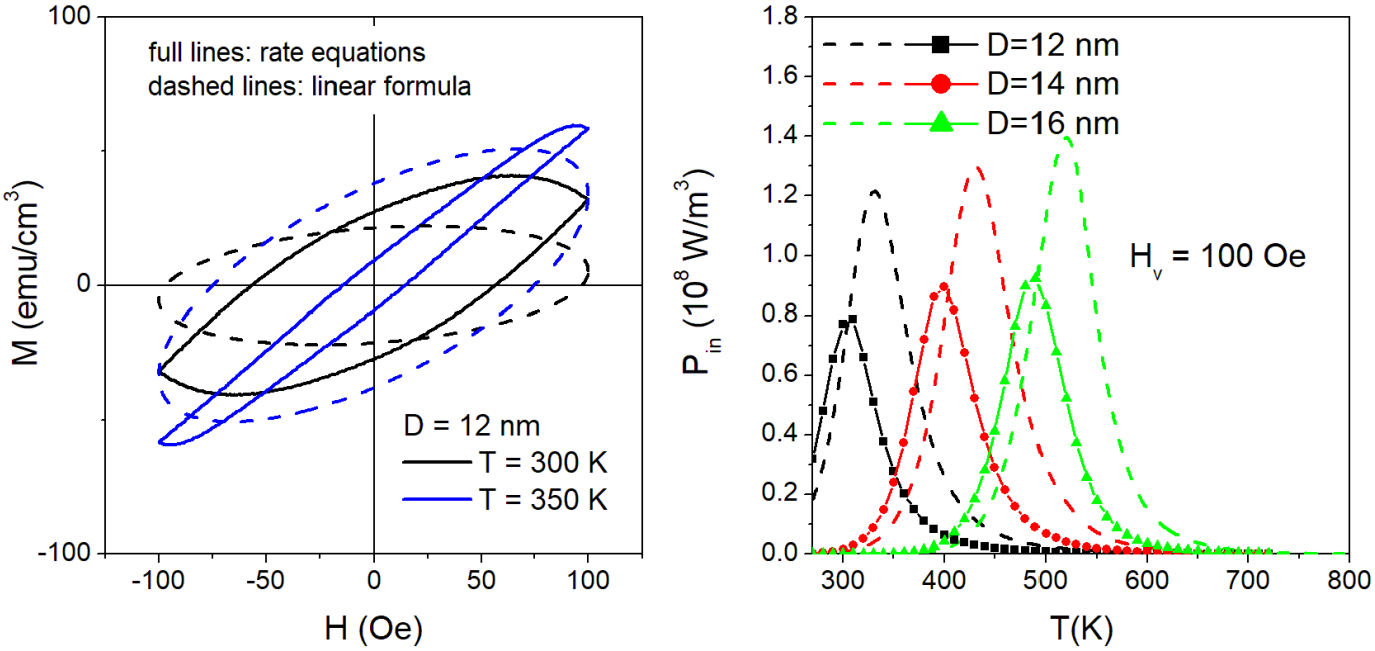

Fig. 9 *(left)* hysteresis loops obtained at two different temperatures by the rate-equation model (full lines) and the linear approximation (dashed lines) for a monodisperse NP system; *(right)* temperature-dependent input power curves obtained by the rate-equation model (connected symbols) and the linear approximation (dashed lines) for three NP diameters.

perature increments, the dependence of the input power on T cannot be safely neglected.

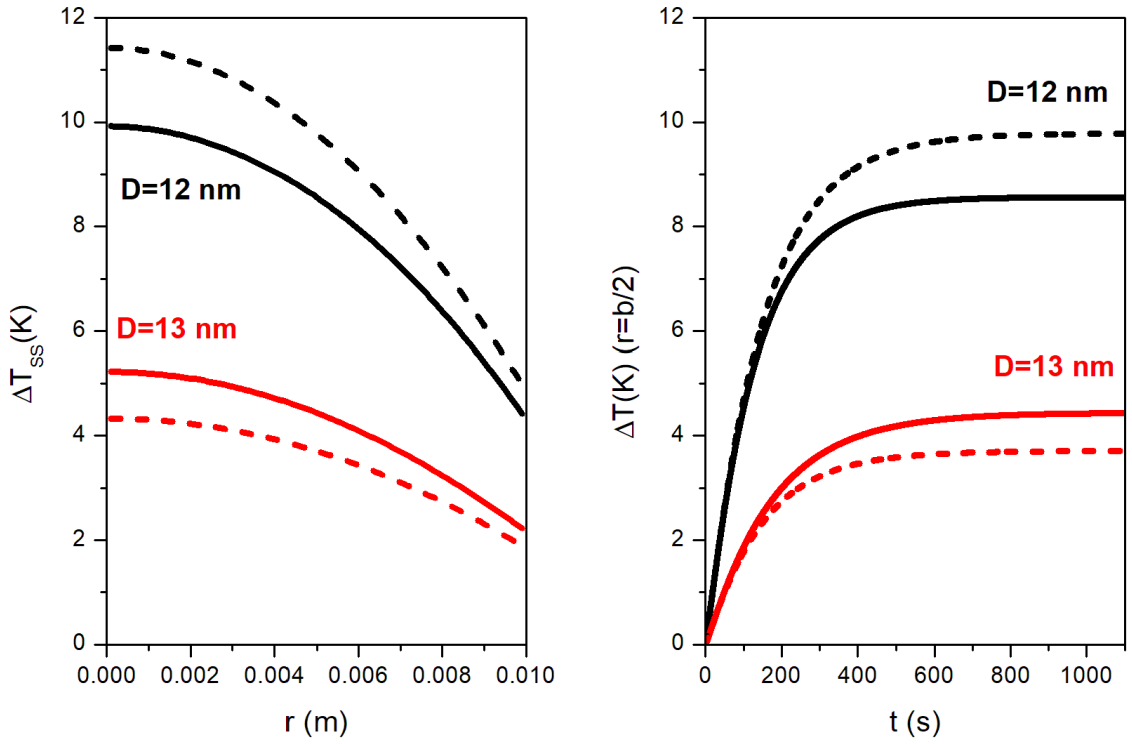

Fig. 10 *(left)* space profile of the steady-state temperature increment for two NP diameters in convective BCs, for temperature-dependent (full lines) and constant (dashed lines) input power; *(right)* corresponding time profiles at $r = b/2$.